FISEVIER

Contents lists available at ScienceDirect

Journal of Volcanology and Geothermal Research

journal homepage: www.elsevier.com/locate/jvolgeores



Variable magma flow in sills: Can a magma source be constrained?

Lauren Hoyer*, Warwick W. Hastie

Geological Sciences, School of Agricultural, Earth and Environmental Sciences, University of KwaZulu-Natal, South Africa



ARTICLE INFO

Article history:
Received 3 June 2021
Received in revised form 15 September 2021
Accepted 8 November 2021
Available online 12 November 2021

Keywords: Magma flow Sill Sill segmentation Dolerite Sill morphology

ABSTRACT

It has been increasingly recognized that emplacement of mafic sills plays an important role in magma transport throughout the crust. However, further understanding of sill propagation and merging of flow within sill complexes in large igneous provinces is needed. This study focuses on outcrop along the KwaZulu-Natal North Coast (South Africa), where dolerite sills of the Karoo Large Igneous Province intruded shales, siltstones, and sandstones of the Permian-aged Vryheid Formation. These sills intruded at high crustal levels and are associated with significant vesiculation, host rock fluidization and brecciation. An integrated approach is used to examine sill morphology, intrusive relationships, and inherent structures in the sills in relation to the magma flow processes. Mesoscale magma flow indicators preserved in the sills include bridge structures, intrusive steps, deformed vesicles, and magma lobes. The predominantly prolate magnetic fabrics determined by anisotropy of magnetic susceptibility techniques indicate magma flow in the sills was oriented NW, NE-SW and SSE, and largely locally coaxial with field evidence. The mesoscale magma flow indicators developed from linkage between numerous sill segments and variation in the magma propagation direction within the plane of intrusion and show directional variation within (and between) sills. The local flow dynamics within each sill can be revealed in this way; however, the possible variation in flow in the intrusion must be considered when interpreting the gross magma flow direction of the entire sill network. The sills occur in close vertical proximity and are inferred to have intruded through lateral and upward magma flow within merging sill segments creating an interconnected sill network, fed from an eastward local magma source. Interpretation of magma flow in sills should be done with care, to avoid oversimplification regarding regional flow, and highly variable flow in sills is best reconciled at the field scale.

© 2021 Elsevier B.V. All rights reserved.

1. Introduction

The magma source of the Jurassic-aged Karoo large igneous province (LIP) has long been argued as a mantle plume, which was traditionally thought to have impacted the base of the lithosphere at the Karoo triple junction, centred on Mwenezi in Zimbabwe (Fig. 1) (e.g. Burke and Dewey, 1973; White and McKenzie, 1989). In addition, the majority of previous structural and magma-flow studies have analysed the dyke swarms which have been interpreted to meet at the Karoo triple junction (Reeves, 1978, 2000; Elburg and Goldberg, 2000; Le Gall et al., 2005; Jourdan et al., 2004; Aubourg et al., 2008; Hastie et al., 2014) with the implication that these developed as the major feeder system to the continental flood basalts. The sills of the Karoo LIP, which have been dated to ~183 Ma (Jourdan et al., 2005, 2007; Svensen et al., 2012), are thought to be the precursor to the continental flood basalts,

however, the Karoo sill system is not wholly understood with respect to the source of the magma and how the magma has migrated in the crust from the source(s).

As the plumbing systems linked to continental flood basalts of LIPs are often inferred to be dyke-dominant feeder networks, with sills traditionally relegated to playing only a minor role in magma transport (Francis, 1982; Lister and Kerr, 1991; Ernst et al., 1995), it is easy to understand how sills have been overlooked in the Karoo system. However, recent work on sills situated away from the Karoo triple junction is emerging (e.g. Galerne et al., 2011; Coetzee and Kisters, 2017; Hoyer and Watkeys, 2016, 2017). It has been shown that sills do not regularly form as extensive tabular intrusions, rather that sills are created through the linkage of previously isolated magma (or sill) segments, which initially have their own propagation direction(s) and dynamics (Pollard et al., 1975; Schofield et al., 2012a; Magee et al., 2016; Galland et al., 2019). In this way, it is possible that numerous sills can link over large geographical areas with magma flow occurring laterally and vertically throughout the sill complex, this is known as an interconnected sill network. Furthermore, recent seismic imaging of sills outside of the Karoo LIP have shown that mafic sills play a major role in the transport of

^{*} Corresponding author. E-mail address: hoyerl@ukzn.ac.za (L. Hoyer).

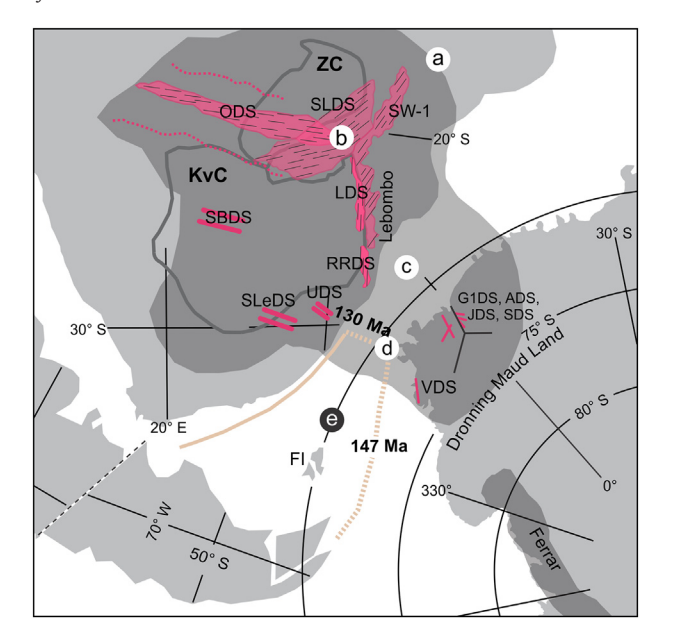


Fig. 1. Basic continental reconstruction of southern Gondwana at circa 170 Ma with the inferred extent of Karoo and Ferrar magmatism (dark grey with dashed white outlines) across southern Africa and Antarctica (KvC = Kaapvaal Craton; ZC = Zimbabwe Craton;FI = Falkland Islands). Major dyke swarms of the region are shown: ODS = Okavango dyke swarm; SLDS = Save-Limpopo dyke swarm; SW-1 = SW-1 (or Mozambique) dyke swarm; LDS = Lebombo dyke swarm; RRDS = Rooi Rand dyke swarm; SBDS = Southern Botswana dyke swarm, SLeDS = Southern Lesotho dyke swarm, UDS = Underberg dyke swarm, VDS = Vestfjella dyke swarm, G1DS = Group 1 dyke swarm, ADS = Alhmannryggen dyke swarm, JDS = Jutulrøra dyke swarm, SDS = Straumsvola dyke swarm. Note that the Antarctic dyke swarms are mainly centred around the Jutulstraumen triple rift in Dronning Maud Land. Regional dyke trends are illustrated with dashes, and the Okavango dyke swarm reaches an overall width of ~300 km (pink dashed line) outside of the densely intruded area (shaded). Later-formed oceanic transform boundaries are shown, with ages of the first known sea floor anomalies The plume positions shown are: (a) from Burke and Dewey (1973), (b) at the Karoo triple junction at Mwenezi, from Burke and Dewey (1973) and Storey (1995), (c) from Cox (1989); White and McKenzie (1989); Storey et al. (1992); White (1997); Curtis et al. (2008), (d) Weddell Sea triple junction from Elliot and Fleming (2000), (e) centre of "megaplume" from Storey and Kyle (1997) (re-drawn from Cox, 1992; Jourdan et al., 2004; Mekonnen, 2004; Ferraccioli et al., 2005; Riley et al., 2006; Curtis et al., 2008; Veevers, 2012).

magma to high-crustal levels and eruptive centres (Marsh, 2004; Thomson and Hutton, 2004; Cartwright and Hansen, 2006; Schofield et al., 2012b, 2015; Muirhead et al., 2012, 2014; Magee et al., 2016; Galland et al., 2018) sometimes as shallow as 500 m in the crust (Airoldi et al., 2011). By linking sills vertically with 3D seismic imaging, Cartwright and Hansen (2006) were able to link deeply-emplaced sills beneath the North Sea with higher-level sills via sill-to-sill junctions, indicating that these become open pathways for upward magma flow; similar work has been completed by Coetzee and Kisters (2017) in sills of the northern part of Karoo basin. Muirhead et al. (2014) expanded on this high-level sill model and showed that a sill-fed dyke network acted as the feeder system to the Kirkpatrick Flood Basalts and high-level magma intrusion in the Ferrar LIP, which is contemporaneous with the Karoo LIP (Fig. 1) (Riley et al., 2006) in South Victoria Land, Antarctica, resulting in a "cracked-lid" appearance.

The study area along the KwaZulu-Natal (KZN) North coast is spatially separate from the saucer-shaped sills in the main Karoo Basin (delineated in Fig. 2) and temporally and spatially distinct from the dyke swarms in the Lebombo volcanic region. It, therefore, presents an opportunity to better understand magma flow during sill intrusion of the Karoo LIP away from previously-constrained magma sources to the north and west. Previous field studies and anisotropy of magnetic susceptibility (AMS) and shape preferred orientation studies of sills in

this area (Hoyer and Watkeys, 2016, 2017) focussed primarily on the results obtained from flow indicators, and comparisons amongst them. This paper presents new data for two additional sills and attempts to more broadly interpret the entire intrusive body in terms of small-scale flow variation, depth of intrusion and the implications of this.

Thus, the aim of this study is to establish, using magma flow indicators, the intrusion dynamics (e.g. depth, intrusion-wall rock interaction, flow directions from melt source) in these sills, and what the implications may be for the understanding of the crustal conditions during sill emplacement in general. Further to this, the results are used to elucidate if a magma source can be constrained when the flow in a sill network is variable, even at a local (tens of metres) scale and whether or not such magma flow can be reconciled with a consistent and geologically reasonable mechanism. Thus, the objectives of the study are to elucidate the magma flow dynamics within thin sills in the eastern portions of the Karoo Basin by determining magma flow directions within the sills, using AMS and field observations, and analysing the factors that affected the flow within these sills when they were forming.

2. Geological setting

The Karoo LIP extends for $\sim 3 \times 10^6$ km² across southern Africa (Eales et al., 1984) and contains numerous volcanic and intrusive components (Cox et al., 1967; Duncan et al., 1984; Ellam et al., 1992). The bulk of the magmatism of the Karoo LIP occurred between ~ 183 Ma and ~ 178 Ma but continued up to ~ 174 Ma as the Lebombo rifted volcanic margin developed (Duncan et al., 1997; Watkeys, 2002; Jourdan et al., 2005; Klausen, 2009). However, the majority of the tholeitic basalt eruption occurred over a period of 3–4.5 Ma (Jourdan et al., 2007), with emplacement of the feeder network of sills in South Africa occurring very rapidly (< 0.9 Ma) at circa 183 Ma (Svensen et al., 2012). Readers are referred to the studies of Erlank (1984), Jourdan et al. (2008) and Hastie et al. (2014) for a more comprehensive synthesis of the Karoo LIP.

The dolerite sills studied here form a portion of the plumbing network of the Karoo LIP that intruded rocks of the Vryheid Formation of the Ecca Group (Karoo Supergroup). The study area is a narrow strip of the KwaZulu-Natal North Coast in South Africa (Fig. 2). Regionally, the geology comprises Proterozoic crystalline basement of the Namaqua-Natal Metamorphic Province (NNMP), which is unconformably overlain by arkosic to quartz-rich sandstone units of the Ordovician Natal Group (Marshall and von Brunn, 1999). A hiatus exists between the Natal Group and the overlying Karoo Supergroup (Johnson et al., 2006), the base of which consists of the glacially-derived Dwyka Group. The Permian Ecca Group overlies the Dwyka Group and comprises marine shales of the Pietermaritzburg Formation, which is overlain by the Vryheid Formation that contains upward-coarsening deltaic lithologies (sandstones and gritstones) and younger fluvial sequences that fine upwards (sandstones, carbonaceous shales, micaceous shales) (Catuneanu et al., 2005). The Beaufort Group, which consists mainly of immature sandstones and shales, overlies this succession but is not locally exposed in outcrop. The uppermost sedimentary units of the Karoo Supergroup are the Molteno, Elliot and Clarens Formations of the Stormberg Group. Thereafter, sedimentation in the basin was arrested with the subsequent eruption of the Karoo LIP flood basalts, when the volcanism occurred, and the associated dolerites intruded. It has been established from coal seam studies in the Vryheid Formation that, at the time of dolerite intrusion, the Vryheid Formation was buried at a depth of 1-2 km (Johnson et al., 2006; Gröcke et al.,

The earliest known work on Karoo dolerite sills of the KZN North Coast is that of Frankel (1969), who described the intrusions in this area as 'Effingham-type' based on geochemical and petrographic evidence, such as the crystalline basement xenoliths. Such xenoliths have not been reported from elsewhere in the volcanic or intrusive record of the Karoo Supergroup and are probably derived from the NNMP (Frankel, 1969).

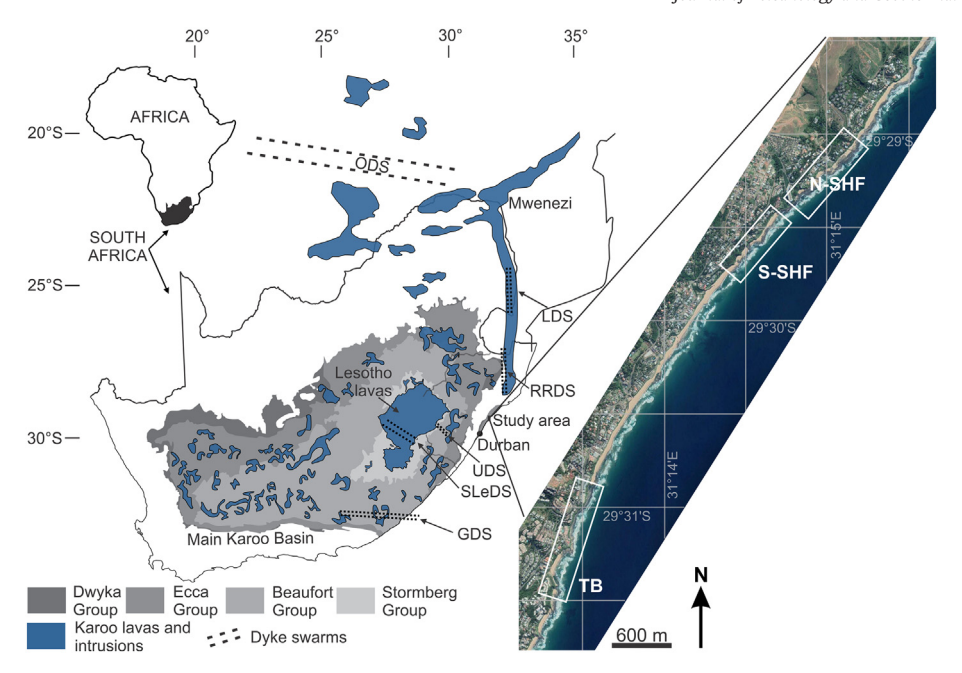


Fig. 2. The erosional extent of the Karoo Supergroup including the sedimentary units, the Karoo basalts and the large-expanse sills in the main Karoo Basin. Dashed lines represent prominent dyke swarms; Okavango Dyke Swarm (ODS), Lebombo Dyke Swarm (LDS), Rooi Rand Dyke Swarm (RRDS), Underberg Dyke Swarm (UDS), Southern Lesotho Dyke Swarm and the Gap Dyke Swarm (GDS). The study area is situated along the KwaZulu-Natal North Coast and separated into three geographic zones; Thompson's Bay (TB) and Southern- and Northern Sheffield (S-SHF and N-SHF, respectively). Modified after Riley et al. (2006) and Hastie et al. (2014).

The study area is divided into three zones based on outcrop availability and extent; the Thompson's Bay zone (TB) in the south and the Sheffield zone in the north, subdivided into Southern (S-SHF) and Northern Sheffield (N-SHF). All sills referred to in this study are described with reference to their geographic area for the sake of clarity.

3. Methods and materials

3.1. Field mapping and sampling

Field mapping of the 8-km-long section of KZN north coast was undertaken, along with photographing and measuring sill orientations and morphologies. Detailed photographs and measurements were made of the small-scale flow-related features, such as ropy flow structures and vesicles, using a declination-corrected compass clinometer (Table 1).

Drill core samples were collected from the margins of the sills. A total of 253 small cylindrical rock core samples (25×25 mm) were drilled out from each margin of the 16 sills using a petroleum-powered, water-cooled rotary core drill (Pomeroy EZ Core Drill by ASC Scientific, Rhode Island, USA). Each core sample was carefully orientated in situ using a Pomeroy OR-2 compass affixed to an aluminium sleeve placed down the drill hole. Between 6 and 10 orientated core samples were taken from a single sill margin, within ~10 cm of the contact (chilled margin) with the country rocks. Only fresh rock was targeted, which was verified later from thin sections of the same sills (Hoyer and Watkeys, 2017), while highly fractured regions of the sills were not sampled to avoid potentially altered rock.

3.2. Magnetic mineralogy

The magnetic properties of the samples were obtained using equipment at the Institute for Rock Magnetism and the University of Minnesota. High temperature analyses were conducted to determine the Curie Temperatures of the magnetic minerals using the Kappabridge High-Temperature Susceptometer. Rock powder samples were heated 700 °C and the susceptibility of the samples measured during heating and cooling.

The MicroMag Vibrating Sample Magnetometer was used to determine magnetic hysteresis (analyses were conducted at room temperature). Domain states of magnetic minerals were inferred by hysteresis properties and may be single domain (SD), pseudo-single domain (PSD) and multiple domain (MD) (Rochette et al., 1999). Samples were exposed to 1 T (T) magnetisation (in 5 mT increments) to obtain hysteresis curves. These data were used to determine the DC Demagnetisation (DCD) results to plot the grain size/domain state of the samples using the Day et al. (1977) and Dunlop (2002) parameters.

3.3. Anisotropy of magnetic susceptibility

Obtaining the AMS has become a standard tool for the analysis of rock fabrics, such as characterising linear and planar fabrics in volcanic, intrusive and metamorphic rocks (Khan, 1962; Ellwood, 1978; Knight and Walker, 1988; Borradaile and Henry, 1997), provided it is determined which magnetic mineral phases are present in the sampled material (Rochette et al., 1999). AMS measurements were obtained using the AGICO Kappabridge MFK1-FA at the Institute for Rock Magnetism at the University of Minnesota via the standard 15 position procedure (Jelinek, 1978). The AMS measurements are represented graphically as an ellipsoid derived from the second-rank susceptibility tensor. The shape, anisotropy and orientation of the magnetic fabric are the most fundamental parameters which can be used to relate the magnetic fabric to the petrofabric (Jelinek, 1981). Readers are referred to Tarling and Hrouda (1993) for a comprehensive overview of the principles of AMS in geological applications.

For studying flow-related fabric in sills, the AMS ellipsoids are determined from the opposing margins (i.e. upper and lower margins) which can provide a constraint on the original magma flow direction (Geoffroy et al., 2002). Given that few samples were collected from the central portions of the sills (and only for TB2 and TB7), we cannot comment on magnetic fabric or flow directions interpreted from AMS in the regions beyond the margins. The AMS data from each sample is then grouped for each site and represented as an ellipsoid in a standard lower hemisphere stereographic projection. The projection shows the

Table 1Orientations of field structures and AMS results.

Sill	Geographical co-ordinates		Strike/Dip	Sill thick-	Type of Magma	Structure	AMS (dec/inc) Upper Contact		AMS (dec/inc) Lower Contact		Inferred Magma	Sill characteristics and the influence
Name	Latitude	Longitude	of Sill	ness (m)	Flow Indicator	Long Axis	Lineation K1	Foliation	Lineation K1	Foliation	Flow Direction	of fluids on the sills
TB1	29° 31′ 39.05″	31° 13′ 41.17″	172°/22°	3.0	ropy-flow structures	216°	275°/08°	218°/14° *	_	-	216°	large vesicles, basement xenoliths
TB2	29° 31′ 14.69″	31° 13′ 42.05″	167°/21°	2.5	elongated vesicles	124° - 304°	168°/01°	256°/14°	157°/39°	069°/87°	~165°	abundant vesicles, amygdaloidal zone
					ropy-flow structure	301°	163°/04° (V)	226°/09° (V)	174°/03° (A)	234°/07° (A)		xenolithic zone, ~5 magma pulses
TB4	29° 31′ 13.87″	31° 13′ 42.87″	172°/25°	1.0	N/A	N/A	298°/06°	226°/18°	285°/06°	211°/20°	~295°	central vesicle stringer
TB5	29° 31′ 25.17″	31° 13′ 39.03″	160°/16°	2.0	bridge structure	127° - 307°	268°/07°	214°/11°	277°/03°	193°/27°	~270°	massive
TB6	29° 31′ 25.71″	31° 13′ 41,21″	164°/13°	unknown	magma lobes	205°/212°	306°/04°	230°/21°	-	-	~209°	fine vesicles
TB7	29° 30′ 50.76″	31° 13′ 54.48″	206°/20°	2.0	N/A	N/A	238°/14°	200°/18°	305°/10°	233°/29°	~294°	vesicles, minor xenoliths
							288°/02°	225°/05°	sill centre			
SHF2	29° 29′ 43.44″	31° 14′ 46.68″	000°/20°	1.0	bridge structures	000° - 180°	172°/37°	246°/66°	275°/02°	200°/07°	172°	central vesicle stringer
SHF3	29° 29′ 41.64″	31° 14′ 46.93″	340°/17°	2.2	bridge structures	163° - 243°	240°/33°	170°/62°	213°/30°	250°/36°	~240°	sediment dykes, amygdales
SHF4	29° 29′ 37.32″	31° 14′ 49.56″	350°/12°	1.5	intrusive step	144° - 324°	323°/05°	031°/12°	155°/12°	103°/18°	323°	massive
SHF5	29° 29′ 41.28″	31° 14.48.48″	353°/30°	1.2	bridge structures	175° - 355°	163°/23°	226°/44°	184°/24°	187°/23°	~174°	massive
SHF6	29° 29′ 32.64″	31° 14′ 57.48″	013°/13°	2.5	bridge structures	324°/031°	276°/04°	000°/30°	087°/01°	000°/21°	276°	sediment dykes, xenoliths, 2 magma pulses
SHF7	29° 29′ 23.64″	31° 15′ 07.56″	056°/10°	>6	magma lobes	055°/060°/064°	294°/02°	211°/13°	132°/12°	163°/14°	~060°	vesicles
SHF8	29° 29′ 19.32″	31° 15′ 10.44″	088°/09°	0.5	bridge structures	~220° - 040°/060°	319°/01°	038°/05°	104°/12°	108°/11°	042°-222°	central vesicle stringer
SHF9	29° 29′ 17.02″	31° 15′ 14.83″	065°/13°	1.5	bridge structures	040 /000 043°/345°	314°/78°	324°/79°	026°/38°	114°/87°	~345°	brecciated host rock, abundant vesicles
SHF10	29° 29′ 14.23″	31° 15′ 17.26″	059°/10°	1	bridge structures	040° - 220°	209°/10°	140°/15°	197°/04°	128°/12°	~210°	massive
SHF11		31° 15′ 24.85″	054°/10°	1.5	bridge structure	145° - 325°	195°/90°	196°/00°	042°/26°	051°/24°	145°-325°	massive

V: vesicular zone.

proportions and orientations of the three principal eigenvectors as $K_1 > K_2 > K_3$ (Jelinek, 1981; Tarling and Hrouda, 1993). AMS studies typically document both linear (defined by K_1) and planar fabric (magnetic foliation plane) elements, which is important when interpreting the orientations of flow-related fabrics relative to the margins of an intrusion. Confidence regions for each of the principal magnetic fabric axes are also developed; in this study the bootstrap method of Tauxe et al. (1998) was used for each principal axis of each ellipsoid (K_1 , K_2 , K_3). Thus, broader confidence ellipses around each axis tend to imply reduced reliability of the interpreted magma flow (described in the next subsection), particularly when the confidence ellipses overlap.

The linear or planar elements are also related to scalar data obtained, including bulk susceptibility $(K_{\rm m})$ corrected degree of anisotropy (P') and shape parameter (T) which aid in interpretation (Jelinek, 1981). For example, the orientation of K_1 may not be coaxial with flow direction when a fabric is of very low susceptibility (Geoffroy et al., 2002) and/or when the fabric is oblate (T>0). In some cases the AMS data may not represent the true petrofabric because of single-domain magnetic mineralogy, or 'inverse' fabrics where K_1 is coaxial with the short grain axis (Rochette et al., 1999; Geoffroy et al., 2002). As such, the interpretation of results presented in this study considers the magnetic mineralogy, confidence regions of principal axes plots, anisotropy (P') and shape (prolate vs. oblate), as well as the orientation of magnetic fabric relative to the sill, described below in terms of magma flow direction.

3.4. Inferring magma flow

Magma flow indicators are morphological structures or structural signatures formed when sills intrude the country rock, specifically where sill segments merge behind a propagating magma front (Pollard et al., 1975; Rickwood, 1990). These have been shown to preserve the initial magma propagation direction (Schofield et al., 2012a; Magee et al., 2018). These structures include intrusive steps and bridge structures (e.g. Nicholson and Pollard, 1985; Kattenhorn and Watkeys, 1995; Hutton, 2009), in the form of broken bridges and bridge stubs, magma lobes or fingers (Schofield et al., 2010, 2012a; Magee et al., 2016, 2018) and deformed vesicles (Liss et al., 2002; Philpotts and Philpotts, 2007). Bridge structures and intrusive steps are planar structures that infer a bidirectional magma flow orientation whereas linear deformed vesicles, which have been elongated in one direction (as observed in 3-D) also indicate a bidirectional magma flow orientation. Deformed vesicles and ropy flow structures are used to infer the sense of magma flow in the intrusions as the formation of these structures is directly related to the mechanisms of magma intrusion, such as propagation and intrusion direction, and local drops in magma pressure (Liss et al., 2002). Ropy flow structures and the termination direction of linear magma lobes infer a unidirectional magma flow direction. These directions or orientations of the inferred magma flow are recorded using the long axes of the structures (Hoyer and Watkeys, 2017).

When magnetic susceptibility is carried by multidomain ferromagnetic minerals (titanomagnetite, magnetite) the resulting AMS ellipsoid

A: amygdaloidal zone.

^{*} Foliation is parallel with ropy-flow structures.

is related to the shape of the grains. In other words, the grain long axis would be coaxial with K_1 (Rochette et al., 1999; Cañón-Tapia, 2001). Such an AMS fabric in an intrusive magma body (sill or dyke) can be considered flow-related when the magnetic lineation K_1 in prolate fabrics is sub-parallel (and preferably imbricated) to the intrusion margins (Borradaile and Gauthier, 2001, 2003). It can also be considered flow-related in oblate fabrics if the foliation plane (to which K_3 is a pole) is close to parallel to the intrusive body and if this foliation is imbricated relative to side walls. In such a case, the absolute vector of flow can be inferred (Rochette et al., 1992; Callot et al., 2004). In cases where imbrication is not present, the magnetic lineation can be used to indicate the flow direction, but not the absolute vector. Relying solely on the orientation of K_1 to indicate flow direction, without considering the fabric characteristics and mesoscale flow indicators, is problematic. This is because in magmatic rocks there is potential interference caused between planar and flow fabrics that renders the meaning of the magnetic lineation doubtful (Aubourg et al., 2002; Callot and Guichet, 2003). This is often evident where confidence regions of K_2 and K_3 overlap forming a false 'foliation' to which K_1 is a pole. As such, we consider the orientation of the K_1 axis along the magnetic foliation (the orientation of which should coincide with the petrofabric) to infer the flow direction, in the manner of Aubourg et al., 2008.

Certainly, magnetic fabrics determined from AMS require cautious interpretation, because *syn-* and post-flow adjustments of cooling magma in a non-Newtonian state can affect the final igneous fabric which develops in an intrusion (Borradaile and Henry, 1997; Rochette et al., 1999; Hastie et al., 2011). It follows that we consider all aspects of the magnetic fabric character and compare the orientations of the field magma flow indicators with the principal directions in the AMS data.

4. Results

4.1. Sill characteristics

The 16 sills sampled in the study area are sub-ophitic to variolitic dolerites ranging in thickness from 0.5 to ~10 m. The host rocks dip at ~10° towards the SE in the Sheffield area (northern part of the study area) and at ~20° towards the WSW in the Thompson's Bay area in the south. The dolerite outcrops are predominantly sills and inclined sheets, the majority of which have intruded along bedding planes. These sills often have complex morphologies (non-planar contacts) and numerous magma flow indicators present along the sill contacts including broken bridge structures, bridge stubs, intrusive steps, ropy flow structures, elongated vesicles and magma lobes. Some of the sills have multiple episodes of magma injection preserved as discrete layers (e.g. Fig. 3a, b). There are only four dykes observed in the study area, all of which strike ~320° (coast perpendicular) and are laterally isolated and < 1-m-thick. One dyke near SHF9 shows a steeply dipping broken bridge, indicating sub-vertical magma flow. Magma lobes occur along the upper contacts of two sills in the field area. These magma lobes are sub-parallel and terminate laterally in a rounded toe forming a linear structure. Intrusive steps occur in a few of the sills (e.g. Fig. 3c), however, the most common magma flow indicators are bridge structures (Fig. 3c, d), which occur in nine sills. The deformation of vesicles in two sills resulted in ropy flow structures and elongated vesicles in TB1 (Fig. 3e) and TB2 (Fig. 3a), where the shearing of the rapidly cooled magma on the underside of the vesicle indicates the direction of magma flow (Fig. 3f). The long axes of intrusive steps and bridge structures are used to indicate magma flow (Fig. 3g and h, respectively), whereas the termination of magma lobes at the 'toe' indicates the primary magma propagation direction. The nature and direction/orientation of the various magma flow indicators are recorded in Table 1. The sill opening direction, where sill segment morphology is preserved, is vertical to sub-vertical for the sills in the field area (Fig. 3c, d).

The abundant bridge structures between sill segments along the KwaZulu-Natal North Coast trend variably, from NW–SE (TB5, SHF4, SHF11), N–S (SHF2, SHF5), NE–SW (SHF3, SHF10), and NW–SE and NE–SW (SHF6, SHF9). The two magma lobes in TB6 indicate flow towards the SW. Three magma lobes in SHF7 suggest flow towards the NE. The deformed vesicles and ropy flow structures in TB1 and TB2 indicate a sense of magma flow from NE to SW in TB1 and from SE to NW in TB2 (Fig. 4a).

In addition to the distinct sill morphologies, eleven of the 16 sills exhibit features other than magma flow indicators, ranging from confined (fluid-assisted) brecciation, rheomorphic sedimentary dykes (Fig. 3d), vesicles (and subsequent amygdales) and entrained xenoliths (Fig. 3a). The xenoliths in the sills comprise basement (NNMP) or country rock material entrained at depth and proximal to the injection site, respectively. The vesicles and amygdales, typically infilled with quartz and/or calcite and/or chlorite, have accumulated in narrow zones in the sill profile. In the majority of the sills (e.g. TB1, TB2 and SHF3) the vesicles are concentrated into distinct zones in the upper portions of the sills (Fig. 3b), however in three sills (TB4, SHF2, SHF8) a vesicle stringer occurs in the centre of the intrusion.

4.2. Field relationships

The host rocks in the field area typically comprise upward-fining sequences, with the base often marked by a thin (< 10-cm-thick) pebble horizon, overlain by coarse sandstones (and gritstones). These sandstones grade into bioturbated siltstones, in turn overlain by shales, which are occasionally capped with thin (< 50-cm-thick) coal seams. The extent of the dolerite intrusions in the field areas is shown on the maps and in the cross-sections for Thompson's Bay (Fig. 4a, b), Southern Sheffield (Fig. 5a, b) and Northern Sheffield (Fig. 6a, b). The faults that occur in the field areas are dominantly coast parallel normal and strike-slip faults, with a range in orientation from 020°-200° to 050°-230° with minimal vertical displacement on the scale of centimetres up to 1-2 m. Therefore, in each field area, the continuity of the stratigraphy is inferred as belonging to discrete coast-parallel fault blocks. In the idealised cross-sections constructed for these areas, the sills are intrusive into various units of the country rocks and are stacked in the stratigraphy and where the stratigraphy is unknown, no assumptions have been made. Even where sills occur in close proximity to one another, the orientations of the magma flow indicators are not always parallel. For example, the ropy flow structures in TB1 (and the magma lobes in the adjacent TB6) are ~90° different to the orientation of the bridge stub along the upper contact of TB5, and these sills occur in a continuous sequence of stratigraphy. Other examples of this abound in the Northern Sheffield area where the magma flow indicators in the sills indicate magma flow to be either ~NE-SW (SHF7, SHF8, SHF10) or ~ NW-SE (SHF9, SHF11) (Fig. 6a). It is important to note here that the sill SHF7 is the highest stratigraphic intrusion in the Sheffield Beach area with the sills cropping out north of this representing a thin slice of the stratigraphy (the coastline here is subparallel to the strike of the units; Fig. 6a). However, the sills to the north and south of SHF7 are not correlated and appear to be distinct intrusions which do not extend laterally from north to south beneath SHF7.

The sills are generally observed to have intruded into shale host rocks where the lower sill contact is commonly in close vertical proximity to a contact between an underlying sandstone and overlying shale. Along many of these sill contacts are zones where the host rock has been deformed during sill intrusion. For example, at SHF9, a zone of brecciated country rock is confined between two vertically and horizontally overlapping sill segments. Hoyer and Watkeys (2016) interpreted this brecciated zone as forming via fluidisation and fragmentation from magma fluid-interaction where comminuted material was laterally displaced within the host rock wedge that was sandwiched between the sill segments. Another example is at SHF3 where a rheomorphic vein in the form of a sandstone dyke cuts across the sill.

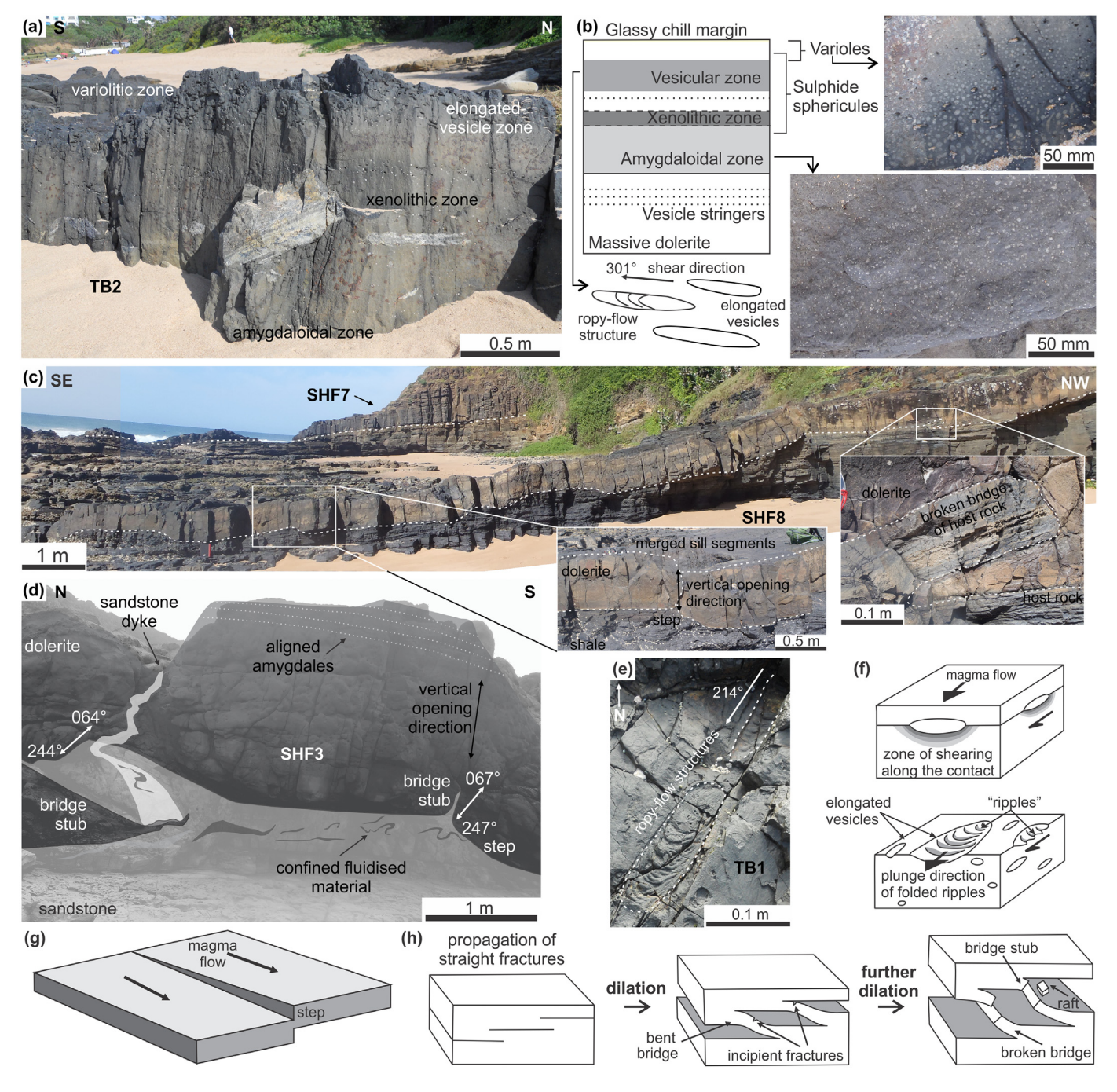


Fig. 3. The common characteristics of sills in the study area. (a) Zone differentiation in TB2 showing the uppermost variolitic zone, the upper vesicular zone and the central xenolithic zone. (b) Stratigraphic column of TB2 showing the discrete zones with photographs of the varioles and amygdales and the orientation of sheared, elongated vesicles. (c) Multiple merged segments that make up SHF8, with the insets showing the nature of the contacts with the hosts rocks where the merged sill segments indicate a vertical opening direction (left inset) and a broken bridge occurs along the lower contact (right inset). Magma flow indicated by these structures is into/out-of the page. Note the sill SHF7 in the background stratigraphically overlying SHF8. (d) Intrusion-induced heating caused fluidisation of the sandstone unit along the lower contact of SHF3 and injection of a sandstone dyke through the sill. Bridge structures along the lower contact infer a ~ WSW-ENE magma flow and a vertical opening direction. Magma flow indicated by these structures is into/out-of the page. (e) To ropy-flow structures that occur 10 cm below the upper contact of TB1. (f) The formation of ropy-flow structures by shearing of magma along the underside of a vesicle (after Liss et al., 2002; Hoyer and Watkeys, 2017). (g) Linking of sill segments that are adjacent can form stepped morphologies (after Pollard et al., 1975; Rickwood, 1990). (h) The propagation of straight fractures can lead to linkage of these fractures, merging sill segments and forming bridge structures (after Nicholson and Pollard, 1985; Kattenhorn and Watkeys, 1995; Hoyer and Watkeys, 2017).

This dyke originates from the bridge stub in the underlying sandstone host rock where portions of partially fluidised host rock are observed (Fig. 3d). Similar features are observed at SHF6 where multiple sediment dykes cross-cut the sill, which originate from the underlying shale units.

Some of the sills show discrete layers through the sill profile (e.g. TB2 in Fig. 3a): (1) an uppermost variolitic unit, where the varioles

have coalesced at the base of the layer; (2) an upper vesicular layer; (3) a central xenolithic layer, where xenoliths are aligned within the layer; (4) a lower amygdaloidal zone with abundant small (~1 mm diameter) amygdales and (5) a lowermost massive layer. There are no chilled margins between the layers but the layers have been differentiated based on noticeable changes in the nature of the layers. Additionally, sill SHF6 comprises two dolerites, with one sill intrusive into the

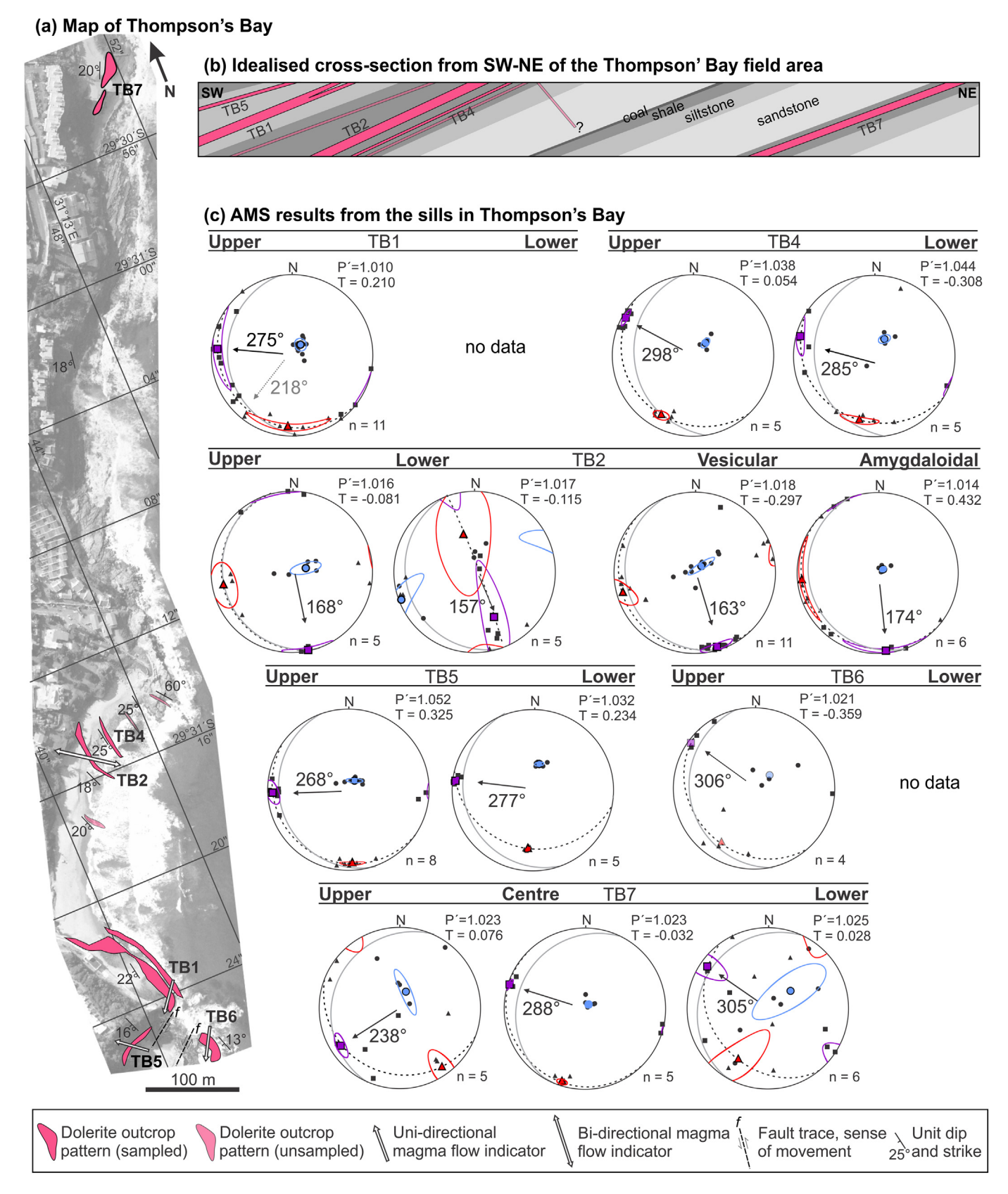


Fig. 4. (a) Simplified geological map of the Thompson's Bay (TB) sills; the outcrop patterns of the dolerite intrusions are shown, and the direction/orientation of the magma flow indicators is shown for each sill. (b) Idealised cross-section from SW to NE of the area showing the stratigraphy of the bay and the relationships between the dolerites and country rocks (not to scale with inaccurate dip angles due to the orientation of the line of section). (c) AMS results from the sill contacts with squares = K1 axis (purple square shows average), black triangles = K2 axis (red triangle shows average) and black circles = K3 axis (blue circle shows average). The coloured ellipses are the 95% confidence ellipses determined for the relevant average K axes. The black dashed lines are the planes of the foliations and the grey B-plane is the original dip and strike of the sill. The arrows and degree values indicate the plunge direction of the average fabric, n = the number of samples, P' is the corrected degree of anisotropy and T is the shape parameter.

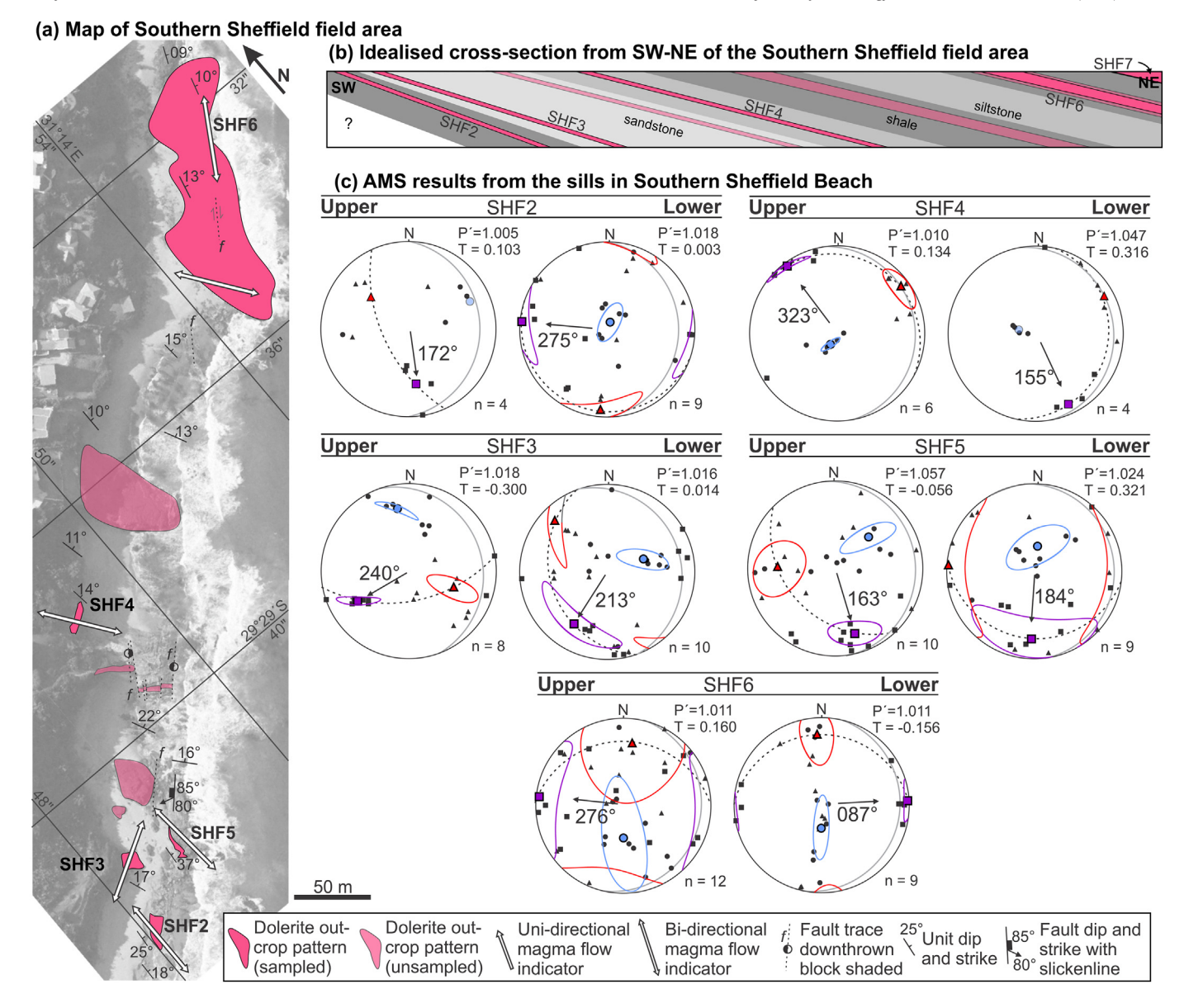


Fig. 5. (a) Simplified geological map of the Southern Sheffield (SHF) sills; the outcrop patterns of the dolerite intrusions are shown, and the direction/orientation of the magma flow indicators is shown for each sill. (b) Idealised cross-section from SW to NE of the area showing the stratigraphy of the bay and the relationships between the dolerites and country rocks (not to scale with inaccurate dip angles due to the orientation of the line of section). (c) AMS results from the sill contacts with squares = K1 axis (purple square shows average), black triangles = K2 axis (red triangle shows average) and black circles = K3 axis (blue circle shows average). The coloured ellipses are the 95% confidence ellipses determined for the relevant average K axes. The black dashed lines are the planes of the foliations and the grey B-plane is the original dip and strike of the sill. The arrows and degree values indicate the plunge direction of the average fabric, n = 1 the number of samples, P' is the corrected degree of anisotropy and T is the shape parameter.

centre or lower portions of the older sill, constrained by the presence of chill margins of the inner sill against the older sill. The magma flow indicators preserved during these two intrusion phases are not the same, with one indicating flow towards the NW and the other towards the NE (Fig. 5a).

4.3. Anisotropy of magnetic susceptibility

The AMS results are shown for each sill separated into different areas; Thompson's Bay (Fig. 4c), Southern Sheffield (Fig. 5c) and Northern Sheffield (Fig. 6c). Some of the characteristics of the AMS fabrics are shown in Fig. 7, including the bulk susceptibility (K_m), corrected degree of anisotropy (P'), shape parameter (T), domains states and high-temperature susceptibility curves. The K_m of the samples analysed ranges between 525 and 13,182 \times 10⁻³ SI, with an average of 4167 \times 10⁻³ SI (Fig. 7a). The P' ranges from 1.001 to 1.210 with an

average of 1.021 (Fig. 7b). The T ranges from strongly oblate (T = 0.846) to strongly prolate (T = -0.842) and indicates that the majority of the samples have prolate fabrics, with an average T of -0.029(Fig. 7c). The main magnetic minerals present are magnetite (5%), marked by a decrease in susceptibility in the samples at the Curie temperature of ~580 °C (Fig. 7d, e). Minor pyrrhotite occurs in most of the sills, marked by a decrease in susceptibility in the samples at the Curie temperature of ~320 °C (Fig. 7d, e). However, the pyrrhotite is interstitial to the silicate fabric (Hoyer and Watkeys, 2017), thus, the AMS signal is carried mainly by magnetite as the dominant magnetic phase. The domain states of the magnetite in the DC demagnetisation (DCD) plot were created using hysteresis data and showed an average pseudosingle domain (PSD) grain size, with the exception being SHF2 plotting above 0.5 on the Mr./Ms. axis showing a single domain (SD) grain size (Fig. 7f) (refer to Hoyer and Watkeys, 2017 for detailed magnetic analysis description).

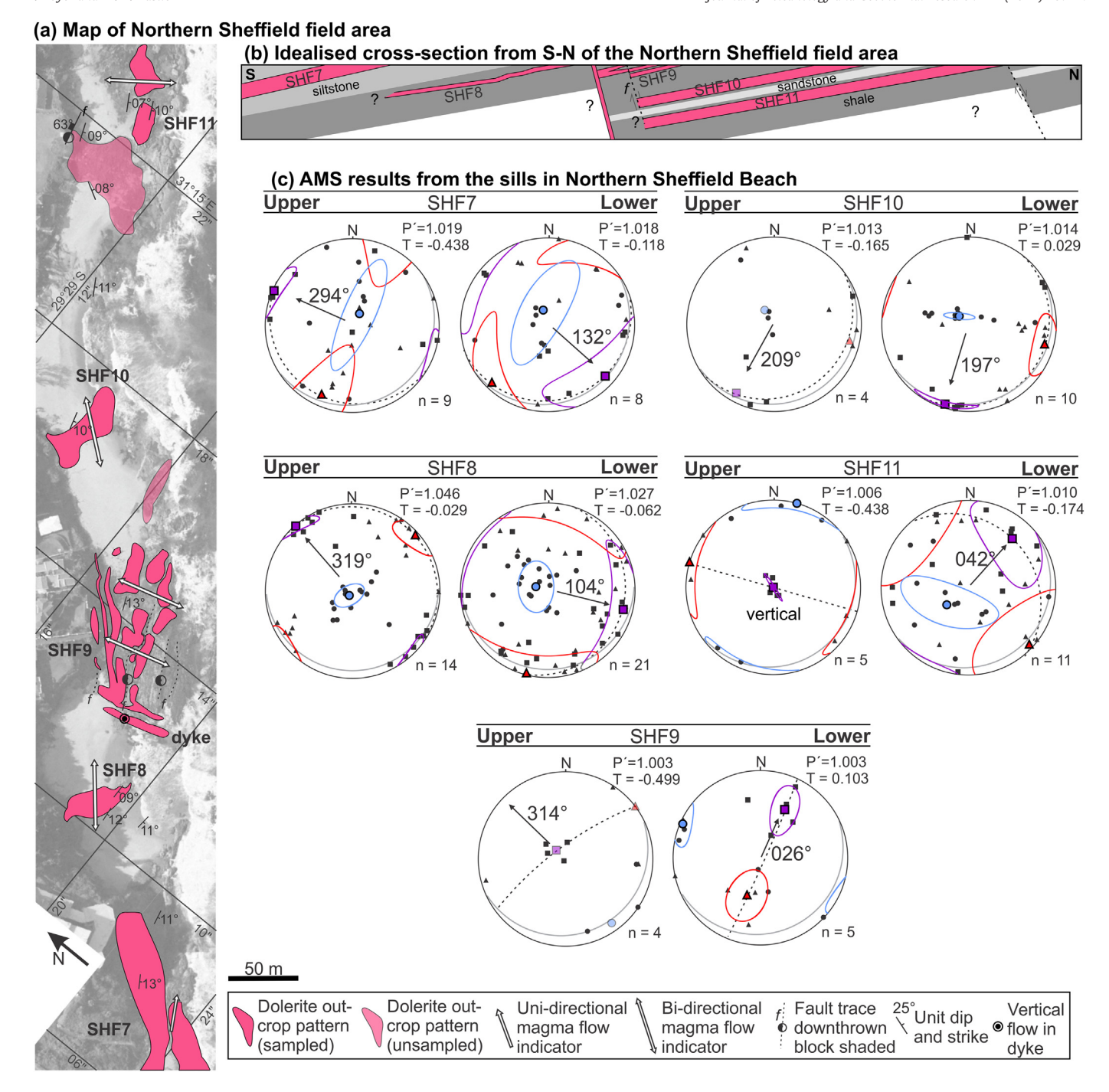


Fig. 6. (a) Simplified geological map of the Northern Sheffield (SHF) sills; the outcrop patterns of the dolerite intrusions are shown, and the direction/orientation of the magma flow indicators is shown for each sill. (b) Idealised cross-section from SW to NE of the area showing the stratigraphy of the bay and the relationships between the dolerites and country rocks (not to scale). (c) AMS results from the sill contacts with squares = K1 axis (purple square shows average), black triangles = K2 axis (red triangle shows average) and black circles = K3 axis (blue circle shows average). The coloured ellipses are the 95% confidence ellipses determined for the relevant average K axes. The black dashed lines are the planes of the foliations and the grey B-plane is the original dip and strike of the sill. The arrows and degree values indicate the plunge direction of the average fabric, n = the number of samples, P' is the corrected degree of anisotropy and T is the shape parameter.

The magnetic foliation plane (represented by dashed lines in Figs. 4–6) are comparable in orientation with the sill orientation in 25 of the 33 margins sampled and is therefore considered to be representative of the actual petrofabric. This is further supported by the lack of single domain magnetic carriers (Fig. 7f) and the well-constrained confidence ellipses in 25 of the 33 margins. However, because we also have magma flow constraints from mesoscale flow structures, it is worthwhile to compare the magnetic fabric (representative of the

petrofabric) to the flow direction(s) inferred from such structures. We classify this comparison as follows: 1) coaxial, 2) perpendicular, 3) poor correlation, or 4) there are no flow structures present.

There are six sills in which the AMS fabric is coaxial with the inherent flow structures where the maximum difference in the direction between the two is <12°; these are TB1, SHF2, SHF3, SHF4, SHF5 and SHF10. The fabric in TB1 is towards 275°, however the foliation dips towards 218°, which is coaxial with the plunge direction of ropy-flow

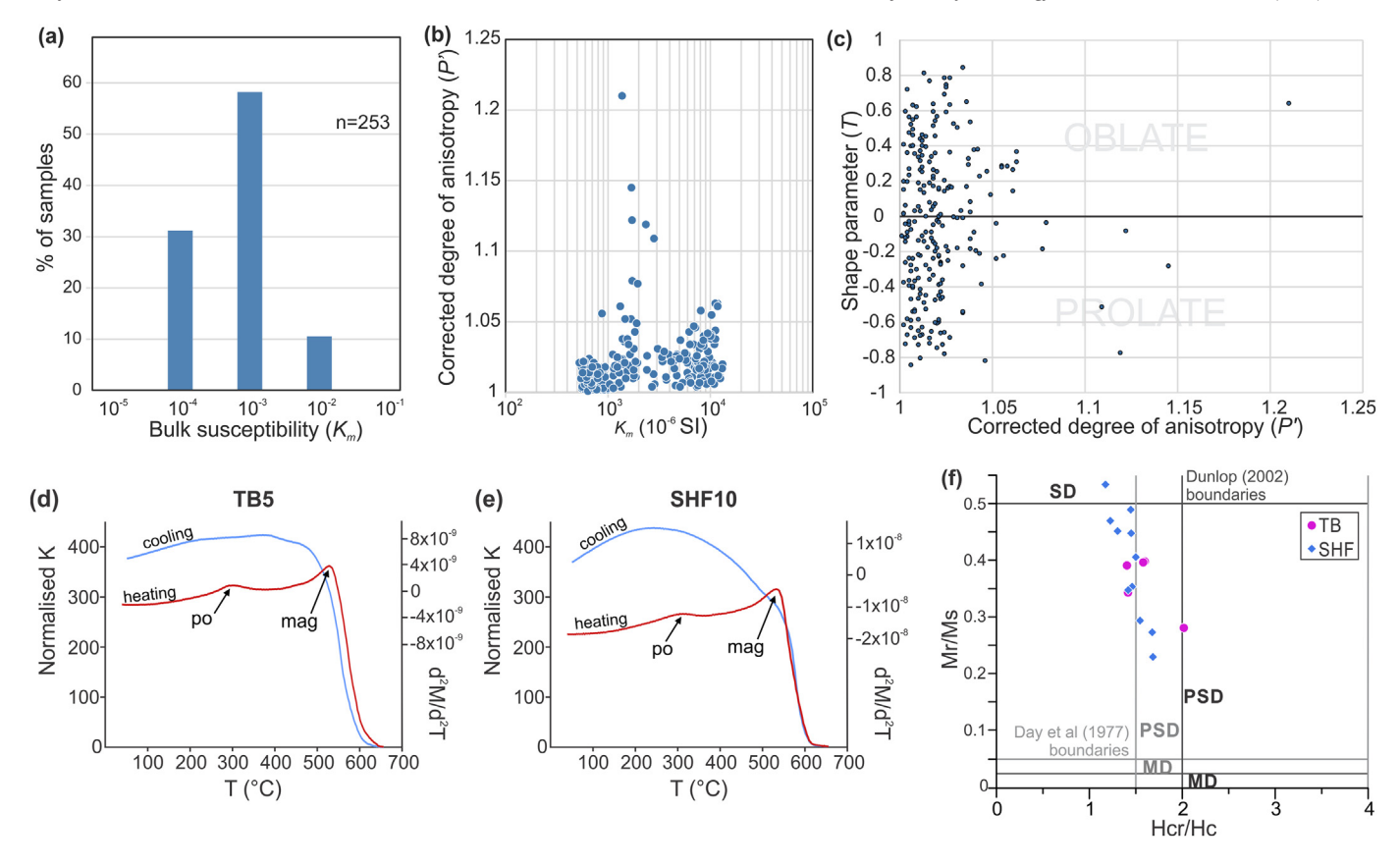


Fig. 7. (a) Bulk susceptibility (Km) histogram for the 253 samples analysed. (b) Plot of the corrected degree of anisotropy (P') and Km. (c) Shape parameter (T) versus P' indicating whether a fabric is prolate or oblate. (d) Susceptibility (K) against temperature (T) for samples from TB5 and (e) SHF10, the heating and cooling curves indicate the dominant magnetic phase is magnetite (mag) with subordinate pyrrhotite (po). (f) Domain states shown on the DCD plot with the Dunlop (2002) and Day et al. (1977) parameters denoting the regions of SD, PSD and MD grain sizes, where samples generally plot in the PSD zone (SHF2 plots in the SD zone).

structures. The AMS fabric of SHF2 and SHF5 are towards the south (172° and 187°, respectively), parallel with bridge stubs. The AMS fabric in SHF3 is orientated towards 240°, coaxial with bridge stubs whilst SHF4 has a fabric orientated towards 155°, parallel with an intrusive step. SHF10 has a magnetic fabric orientated towards 209°, which is parallel to its bridge stub.

There are three sills in which the AMS fabrics are perpendicular to the orientations of the flow structures: TB6, SHF7 and SHF8. TB6 magma lobes plunge towards ~209°, whereas the AMS fabric lineation plunges towards 306°. In SHF7, the magma lobes plunge towards ~060°, whereas the fabric plunges towards the west. The several bridge structures along SHF8 trend ~042°–222°, whereas the AMS fabric lineation plunges to the NW.

There are five sills in which the AMS fabric orientations are distinct from the mesoscale magma flow indicators: TB2, TB5, SHF6, SHF9 and SHF11. Sill TB2 has internally consistent AMS orientations across the vesicular and amygdaloidal zones and the upper and lower contacts, with a SSE-trending flow direction inferred. This differs from the orientation of the elongated vesicles within the vesicular layer plunging on average towards 304°, which is almost identical to the verging direction of a single ropy flow structure (301°). Sill TB5 has a small bridge structure along the upper contact of the sill, oriented with a trend of NW-SE, however, the AMS fabric plunges E-W differing in direction by 30°-40°. SHF6 contains two directions of bridge structures at opposite ends of the intrusion: one NW-trending (324°) in the south on the lower contact of the inner (or internal) sill and the other NE-trending (041°) in the north between the sill and the country rock, which both differ from the AMS fabric that plunges towards the west but is poorly constrained. Sill SHF9 contains several coaxial bridge structures plunging towards ~333°, however, the magnetic fabric is steeply inclined for the upper contact and deviates from the orientation of the bridge structures by 31°. The foliation and lineation of the magnetic fabric from SHF11 along the upper contact are vertical and the fabric from the lower contact does not correspond with the orientation of the bridge structure (145°).

There were two sills sampled which lack inherent flow structures: TB4 and TB7. TB4 has internally consistent AMS results plunging towards 285°–298°. TB7 yields AMS data with a range of directions (238°–305°), but with relatively internally consistent directions (288° and 305°).

5. Discussion

5.1. High level intrusions

In a number of sills in the study area, there are zoned sections evident in profile, such as the vesicular zones in TB1 and TB2 (Fig. 3b) which require examination in terms of magma dynamics and depth during intrusion. Vesicles can form from pressure decreases in the magma resulting from the exsolution of incompatible volatile phases, such as the crystallization of the anhydrous phases pyroxene and plagioclase (Peck, 1978). This leads to fluid-magma separation and vesicle nucleation occurs. The abundant vesicles and entrained crystalline xenoliths that occur in many of the sills studied indicate that the magma was relatively volatile-rich (and therefore buoyant), which was able to migrate to shallow depths relative to a volatile-deficient magma (Menand, 2011; Aragón et al., 2018). The abundant vesicles and amygdales in these sills are characteristic of sills confined to a coast-bound geographically narrow belt (~50 km wide) along the KZN North Coast (Frankel, 1969). Either there was an abnormal volatile

content in the melt, or these sills intruded into lithologies that contained abundant pore fluids. The increased volatile component can be linked to the xenolith content of some of the sills, as volatile-rich magma has a higher capacity for entraining xenoliths (Lensky et al., 2006), some of which are crystalline basement granitoids of the NNMP. Frankel (1969) suggested that the appearance of basement xenoliths rather than country rock xenoliths resulted from stoping of the basement within a shallow magma chamber or intrusion along active faults in the basement. Significant volatiles have also led to fluidisation of clastic rocks upon intrusion, such as in SHF3 (Fig. 3d). The dolerite breccia in SHF9 may also indicate that intrusion occurred at a high crustal level (Hoyer and Watkeys, 2016), as failure of wall rocks around an intrusion, and brecciation and fluidization observed at sill-wall rock contacts has been observed in other parts of the Karoo as a relatively shallow process (Jamtveit et al., 2004; Schofield et al., 2010). This is in agreement with the relatively shallow burial depth of the Vryheid Formation (1-2 km) at the time of intrusion (Johnson et al., 2006; Gröcke et al., 2009).

5.2. Sill emplacement and magma flow directions

Sill complexes are increasingly being recognized as a means for determining tectonomagmatic regimes in LIPs, over and above dykes and dyke swarms (Airoldi et al., 2011; Magee et al., 2016; Stephens et al., 2017). The original magma propagation direction, and potentially the source of the magma, can be inferred by magma flow indicators (Nicholson and Pollard, 1985; Rickwood, 1990; Magee et al., 2018) and AMS analyses, if the fabrics are the product of magma flow (Ellwood, 1978; Philpotts and Philpotts, 2007; Aubourg et al., 2008). However, it is evident that magma flow in sills is far more complex than in dykes because of processes such as magma lobe coalescence and linking of adjacent and/or overlapping sill segments (Magee et al., 2016; Chanceaux and Menand, 2016; Coetzee and Kisters, 2017).

Sill formation is, in general, scale-independent and results from the coalescence of numerous magma segments, a process which typically occurs proximal to the source, followed by separation at some distance from the source (Pollard et al., 1975; Delaney and Pollard, 1981; Schofield et al., 2012b; Magee et al., 2016, 2018). Given that the orientations of planar magma intrusions in the Earth's crust are typically controlled by far-field tectonic stresses (Stephens et al., 2017) and are emplaced orthogonal to σ_3 (minimum compressive stress), it suggests that such flat-lying sills intrude in tectonic regimes where σ_3 is vertical (Anderson, 1936, 1951; Gudmundsson, 2011; Muirhead et al., 2015). However, sills associated with LIPs often form in undeformed basins or at during the initial stages of rifting where σ_3 would be horizontal (Galland et al., 2018). In undeformed areas where magma pressure exceeds local lithostatic pressure (overburden), tensile fractures develop parallel to bedding to allow sill intrusion (Burchardt, 2008). Regional (and local) stress is not the only mechanism responsible for sill intrusion as other factors can affect injection dynamics, such as variations in lithologies and their rigidity and, the presence of pre-existing fractures and/or foliations (Menand, 2011), the effects of which can be complex to interpret. Furthermore, the coalescence of overlapping and initially unconnected magma segments (sill segments) can occur due to a local rotation of the principal stress directions in the interaction zone between offset segments (e.g. Pollard et al., 1982; Nicholson and Pollard, 1985; Cooke and Pollard, 1996; Cooke et al., 1999; Burchardt, 2008) or by magma making use of pre-existing structures or weaknesses in the host rock (e.g. Baer et al., 1994; Jolly and Sanderson, 1997; Hutton, 2009; Schofield et al., 2012a; Stephens et al., 2017) or a combination of both.

We have demonstrated on the KZN North Coast that 12 of the 16 dolerite sills studied have overlapping morphologies, and are connected, as evidenced by steps, bridges and bridge stubs. The sills are relatively thin, but extensive sheets and virtually all connectors between sills are inclined sheets, not dykes. The linking of sill segments resulted in the formation of bridge structures and intrusive steps in 12 of the 16 sills in the

study area (bridge structures in TB5, SHF2, SHF3, SHF5, SHF6, SHF8, SHF9, SHF10, SHF11; intrusive steps in SHF4 and magma lobes in TB6, SHF7) where overlapping sill segments merge and country rock is deformed between segments.

As described earlier, we interpret AMS fabrics with caution, for several reasons. Firstly, recording of magma flow is affected by internal processes (magma pulses or convection) (Benn and Allard, 1989; Paterson et al., 1998) and magmatic fabrics are typically representative of the last stages of strain during magma injection and crystallization. As such, it is not uncommon to find late-stage compaction of fabrics (Park et al., 1988; Philpotts and Philpotts, 2007) or late changes in bulk flow direction (Paterson et al., 1998; Aubourg et al., 2002) which may alter particle rotation, and thus the magnetic fabric and petrofabric. Therefore, we consider here the AMS fabrics as representative of the magma flow directions where the AMS fabrics and the magma flow indicators are coaxial, as is the case for TB1 (218°), SHF2 (172°), SHF3 (240°), SHF4 (323°), SHF5 (174°) and SHF10 (209°) (Fig. 8). The AMS fabric is used to infer the magma flow for TB5 where the data are coaxial across the sill contacts and is similar in orientation to the magma flow indicator (272°), or where there are no mesoscale structures present in TB4 (291°) and TB7 (296°). However, there are discrepancies between the AMS fabrics and magma flow indicators in sills TB2, TB6, SHF6, SHF7, SHF8, SHF9 and SHF11 (Fig. 8). Where the AMS fabric is perpendicular to the orientation of the magma flow indicators, this may be due to disruption of the fabric when parallel magma segments merge laterally (see Hoyer and Watkeys, 2017 for detailed discussion). Therefore, the primary magma propagation directions are inferred using the direction/orientation of the mesoscale structures in these sills: TB6 (209°), SHF7 (060°), SHF8 (042°-222°), SHF9 (333°), SHF11 (145°-325°) (Fig. 8).

The sill TB2 requires special attention as it is separated into discrete zones based on varying characteristics in terms of vesicles and xenolith content. It is unlikely that these layers are the product of in situ gravitational differentiation as the base of certain layers can be differentiated from the top of the lower layer, notably in the variolitic layer where varioles coalesced at the base of the layer by density settling (Fig. 3a, b). The presence of these layers indicates that multiple pulses of magma were injected in close succession, prior to cooling of the magma as no chill margins formed. If these layers were injected from the same magma source, it appears to have been heterogeneous in terms of the volatile content, with some volatile-rich pulses entraining large xenoliths during transport (Lensky et al., 2006; Yoshinobu et al., 2009). In the sampled layers of TB2 the AMS fabric is consistent across the various zones, but these fabrics are not parallel with the shearing direction implied by the deformed vesicles (Fig. 8), which most likely formed as a direct product of shear from magma flow (Liss et al., 2002; Philpotts and Philpotts, 2007). It is possible that thermally induced resetting of AMS carrier minerals occurred because of multiple magma injections that formed the layers of different characteristics. This thermal resetting (Henry et al., 2003; Hastie et al., 2011) would have aligned the AMS fabrics to a common direction and may have occurred more than once based on the nature of the intrusion. This may be true of TB6, SHF6, SHF7 and SHF9 as well. The two differently oriented bridge structures in sills SHF6, for example, could have resulted from magma injection during subsequent magma pulses, which were locally propagating in different directions within the sill, whilst still dilating perpendicular to σ_3 (Stephens et al., 2017) (discussed further in Section 5.3).

If all evidence of flow is considered (see integrated flow indicators in Fig. 8) in the structural context of the sills, it is evident that: (1) where the sills are clearly the result of several overlapping and merged sill segments (lobes and bridge structures), such as TB6, SHF6, SHF7 and SHF8, these structures represent the initial magma propagation direction of the sills (Schofield et al., 2012a; Hoyer and Watkeys, 2017; Magee et al., 2018); (2) the orientations of bridge, lobe and flow structures are consistent with bi-directional magma flow along NW–SE and NE–

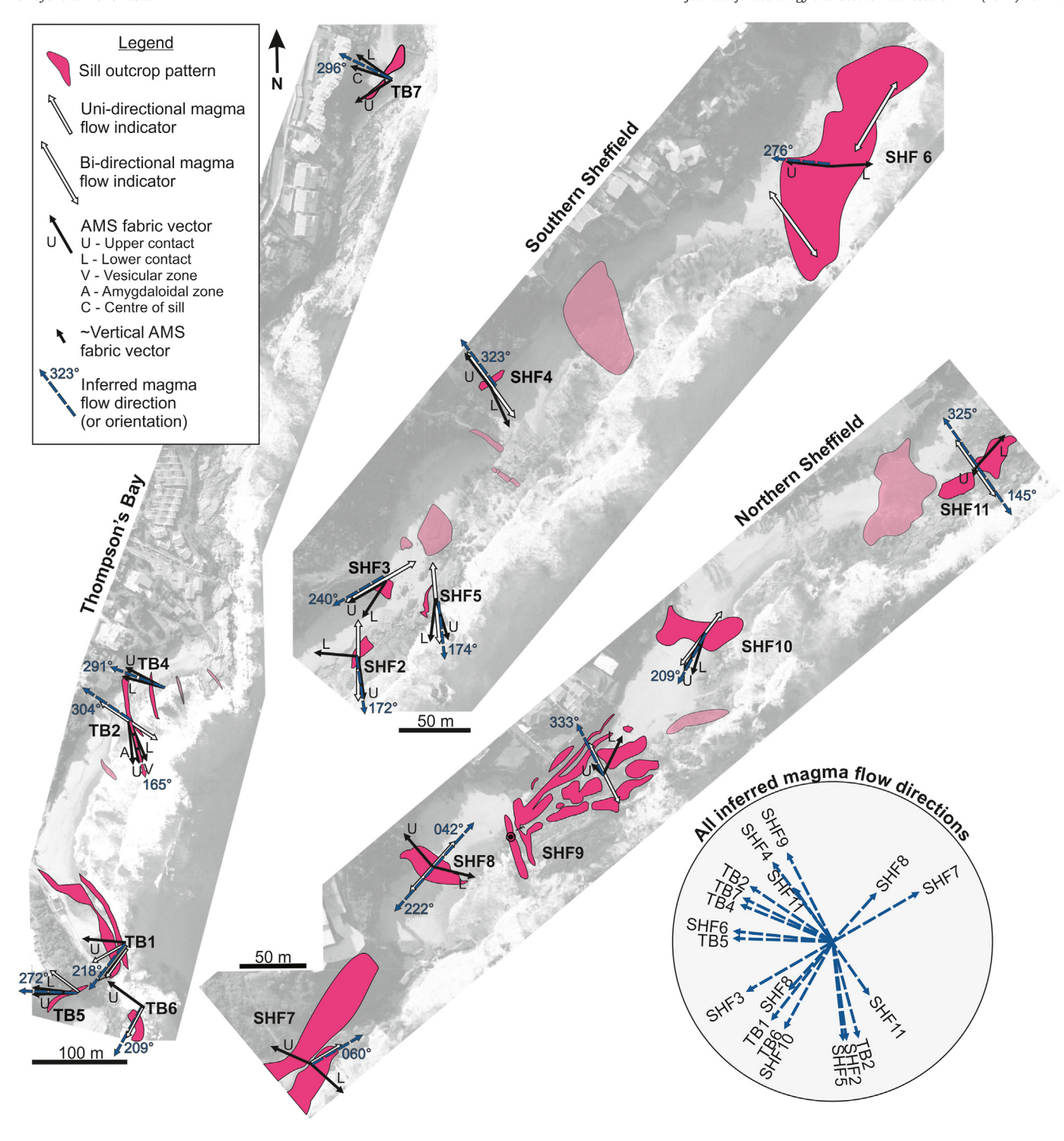


Fig. 8. Integrated flow direction results from field structural evidence (uni- and bi-directional white arrows) and from AMS fabrics (black uni-directional arrows) for the 16 sills on the KwaZulu-Natal North Coast. The dashed blue arrows represent the inferred magma flow direction for each sill, summarised in the grey rose diagram). Note the relationships between the AMS fabrics and magma flow indicators, which are coaxial (TB1, TB4, TB7, SH2, SH3, SH4, SH5, SHF10) and non-coaxial (TB2, TB5, TB6, SHF6, SHF7, SHF9, SHF911).

SW orientations and unidirectional flow towards the NW and NE (Fig. 8); and (3) these same directions are recorded in the magnetic fabric of certain sills (NE in SHF9, SHF11; SW in SHF3 and NW in TB4, TB6, TB7, SHF4, SHF7, SHF8).

5.3. Implications of variable magma flow indicators

While the variation in magma flow indicators, as discussed above, is expected in a natural magmatic system, it is evident from this study that

amongst sills (and even within some sills), there are inconsistencies, to the extent that an array of magma injection orientations has been measured: the cluster around magma flow towards the NW, SSE and along a NE–SW axis (Fig. 8). Here we explore the reasons for such variability and the implications when trying to understand magma dynamics in the plumbing systems of LIPs.

Firstly, if we consider the sills as a component of the Karoo LIP and attempt to understand large-scale (or long-range) magma transport, it may be tempting to infer a link to a mantle plume (or least a point

source) as has been done previously (Burke and Dewey, 1973; White and McKenzie, 1989; Storey, 1995). For example, one might consider the position of the study area, and certain sills which intruded from the southeast (SHF4, SHF6, SHF9, SHF11, TB2, TB4, TB5, TB7), to be consistent with the plume position (d) in Fig. 1 (Elliot and Fleming, 2000). However, this does not accord with the intrusion directions of the other 11 sills, and also belies the overall spread in recorded magma flow directions at the local scale (Fig. 8). For example, SHF3 and SHF4 have coaxial magnetic fabric, and reliable flow indicators, yet have flow orthogonal to each other. Similar findings have been made and reviewed regarding dyke swarms of the Karoo LIP which suggest that interpretation of magma flow directions with the aim of elucidating large-scale transport is ill-advised without considering the local effects (e.g. tectonic regime, structural architecture of the host rock) (Ernst and Buchan, 1997; Le Gall et al., 2005; Hastie et al., 2014). It therefore is not reasonable to infer a single 'point' source at the regional scale for our findings, nor is it reasonable to infer separate sources, and separate events for each of the flow directions.

Instead, it is worth considering our observations of the sills and host rock in the field (i.e., local-scale architecture) and previous work that has examined magma flow in sills. For example, as sill segments or lobes migrate through the lithosphere, they merge to create larger sheets (Hansen et al., 2011). As they merge, portions of deformed host rock are captured by the sills or remain in situ (particularly at the termination of the segments/sill). The primary linkage direction is in the horizontal plane, perpendicular to the predominant magma flow. As with saucer-shaped sills, the propagation direction can shift from horizontal to sub-vertical (thus forming inclined sheets) (Coetzee and Kisters, 2018), which has been documented as a mechanism of sill intrusion elsewhere (e.g. Thomson and Hutton, 2004; Burchardt, 2008).

In terms of magma flow dynamics within sills, there is another explanation. When multiple lobes are injected into the same crustal level from one feeder source it is possible that the flow orientation changes depending on the propagation direction of the various lobes (Fig. 9a, b). With a central pipe-like feeder source, magma flow into the country rocks from that source can create circular-shaped sills (Chanceaux and

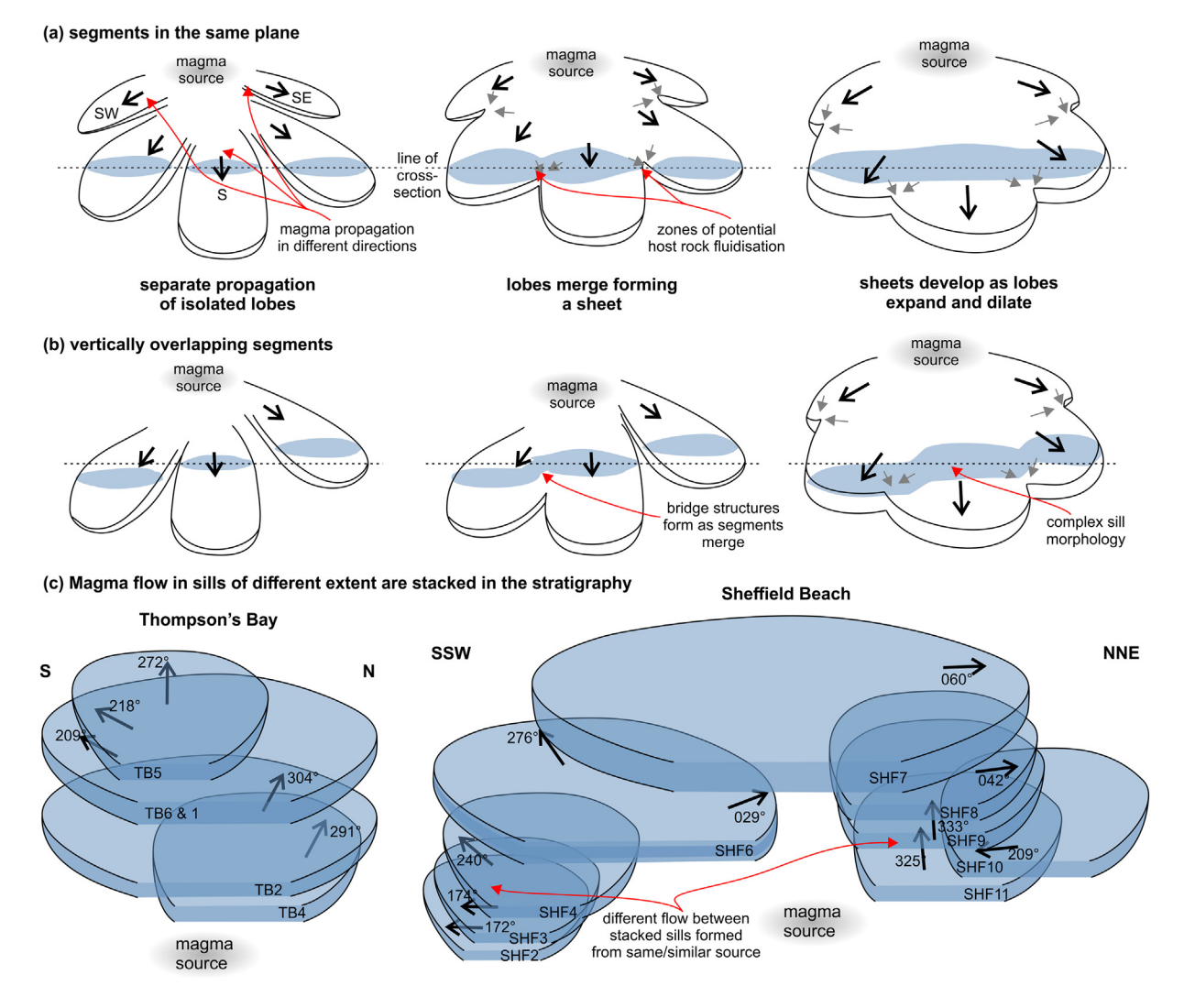


Fig. 9. Intrusion dynamics of magma lobes in sills. (a) Sill segments occur in the same horizontal plane, which inflate and merge to form relatively flat-lying sheets. With the merging lobes, magma flow indicators that are preserved where these segments merge, may indicate different directions of flow on either side of the circular sheet. In cross-sectional view the sill segments merge to form one seemingly homogenous sheet (blue shapes). (b) Sill segments occur at different stratigraphic levels and merge to create steeped morphologies in an interconnected network. In cross-sectional view the sill segments merge to form steps in sheets (blue shapes). In (a) and (b) the large black arrows indicate the magma flow direction in each lobe and the small grey arrows indicate local flow between merging segments. (c) When multiple sills are stacked in the stratigraphy, the preserved magma flow directions may not be consistent depending on the size of the circular sills, resulting in what appears to be a variation in the magma source. Here the results for the sills from Thompson's Bay and Sheffield Beach indicate that they may have been fed from a local magma source located to the east of their current locations.

Menand, 2016). If the sill is more circular, with restricted flow in propagating lobes (i.e., stubby lobes), and an overall radial and lateral flow from a proximal source, variability in the magma flow within one sill can be variable (Fig. 9). As magma lobe terminations or closure directions can show the direction of outward sill propagation (Schofield et al., 2012a; Magee et al., 2016), where there are two differently oriented magma flow indicators at different ends of a sill (such as two bridge structures in SHF6 that exhibit orthogonal directions; NW-SE and NE-SW), this may indicate that lateral magma migration was inhibited, and dilation and merging of sill segments allowed for sill growth (Fig. 9a, b). Magma flow would therefore not be consistent across the sheet, which could have a flat-lying (Fig. 9a) or a stepped morphology depending on the arrangement of the sill segments prior to merging (Fig. 9b). This has been documented in both 3D seismic data of sills (Thomson and Hutton, 2004; Schofield et al., 2012b; Magee et al., 2015) and analog models of sills (Kavanagh et al., 2017; Chanceaux and Menand, 2016) or where there is a clear 3D relationship between lobes of the same sill (Horsman et al., 2005; Wilson et al., 2019).

If an inclined sheet developed upwards, but is oriented perpendicular to the primary flow direction, two sill segments would become linked (the lower segment merging with the upper in this example) (see Fig. 3g, h), but flow within the inclined sheet would be perpendicular to the overall flow. It will depend on the stresses imposed on these segments that will determine where and how they will link. In these scenarios, outward magma flow is limited, indicating that there is little variation between σ_1 and σ_2 within the horizontal plane (Stephens et al., 2017). When observing cross-sections of these stacked sequences in the field, their limited exposure dictates the direction of magma flow that can be measured from the mesoscale indicators, but any variation in local magma flow direction in each of the merged sill segments can be reconciled with a discrete local magma source (as has been modelled by Chanceaux and Menand, 2016) if the local sill geometry and architecture is considered (Fig. 9c).

Extrapolation of magma flow directions from the two geographically separate field areas suggest that the source of the magma was a central pipe-like feeder located eastward of Thompson's Bay and Sheffield Beach (Fig. 9c). Depending on the proximity of the magma origin to the area, the sills may have been sourced from eastward of the present coastline, possibly the Weddell Sea triple junction as located by Elliot and Fleming (2000) (Fig. 1).

The sills studied on the KZN North Coast have evidence of (1) fluidization and brecciation of the host rocks, (2) vesicular and xenolithic character, occasionally with vertical zoning thereof (3) variation in the directions of magma flow within (a) individual sills and (b) between sills stacked in the stratigraphy. Taking these factors into account, it can be argued that a relatively coherent mechanism was responsible. We propose that the development of segments between sills not only facilitated lateral and upward magma migration, but also resulted in pressure reductions which led to vesicle formation and, along with heating of pore fluids during intrusion, assisted in fluidization and related brecciation, all of which occurred at relatively high crustal levels, as shown in similar studies in the main Karoo basin (e.g. Jamtveit et al., 2004; Schofield et al., 2010). In addition, the magma flow within the sills is variable due to the nature of formation of sills into sheets where multiple lobes can merge, either in the same plane or overlapping. As such, the pattern of magma flow across multiple sills in an area is complex and poses challenges in inferring a magma source.

Thus, it is likely that these sills developed from a local magma source (s) where inclined sheets or small dykes connect with sills laterally and vertically, operating as open conduits from depth to near-surface (i.e., stratigraphically elevated sills in the Vryheid Formation). Such a situation is consistent with other sill complexes where vertical inflation of sills and a strong degree of interconnectedness has been observed (Cartwright and Hansen, 2006; Muirhead et al., 2012, 2014). Interconnected sill networks with apparently variable intrusion geometries have been found elsewhere in the Karoo basin (Coetzee and Kisters,

2017), and are known to have the capacity for magma transport over large lateral distances (Cartwright and Hansen, 2006; Magee et al., 2016)

Sills of this study accord well with an interconnected system of sills feeding sills, with merged sill segments acting as the connectors (and open conduits) that are not feeder dykes, implying an upward and lateral magma migration within the complex (e.g. Airoldi et al., 2011; Muirhead et al., 2014). The dynamics of a sill system such as the one studied here are complex and the resulting magma flow directions determined for the 16 sills may simply represent the magma flow that occurred in the area of the sill, which is currently exposed in the field. The regional magma flow regime is therefore difficult to constrain. What is clear is that the magma flow dynamics within the sills of the Karoo LIP could be different depending on where they occur within the Karoo basin and may represent intricate relationships between magma intrusion, host rock deformation and indicating the magma source.

6. Conclusions

The underrepresentation of sills in the scheme of magma transport and feeders to continental flood basalts is coming to an end. In more areas, it is being shown that dykes are not the principal feeder to LIPs and that interconnected networks of sills extending from the magma source to high-crustal levels are the primary system of magma transport in the crust.

In this study, we have shown that the magma flow in sills along the KZN North Coast of South Africa have preserved multiple magma flow directions/orientations. These primary magma flow orientations are NW, NE–SW and SSE and were determined using AMS and mesoscale structures resulting from magma flow. The variation of the magma flow in the sills together with evidence of vesicles, fluidization and localized brecciation, indicate that the sills along this stretch of coastline were intruded at a higher-crustal level than the sills in the equivalent Ecca Group units in the main Karoo Basin.

This study shows that understanding the dynamics of sill intrusion and propagation can be difficult, even with good exposures at the local scale. For example, the magma flow indicated by the mesoscale structures and the AMS analyses in this study may not represent the finite or absolute magma flow dynamics within the entire sill network, but rather reflects something of the mechanism of intrusion and coalescence: If merging sill segments cannot extend laterally within the horizontal plane whilst intruding, magma injection is accommodated by sill inflation and segment linkage. This process forms circular sills and creates differently oriented magma flow indicators (and different magma propagation directions) where lobes have merged on opposite sides of circular sills, creating an apparent variation in the magma source. As such, the magma source inferred for these sills was located to the east of the present coastline.

Although a magma flow direction can be defined for each sill in the study area, these directions may not represent a regional flow regime but rather local flow in isolated portions of sills, which can be variable within the intrusion. As such, future studies of sill intrusion, regardless of outcrop quality and availability, should be cautious of large-scale interpretation, but rather be aware that results may reveal local-scale intricacies of magma injection, pulses, and segment merging.

Declaration of Competing Interest

The authors declare that they have no known competing financial interests or personal relationships that could have appeared to influence the work reported in this paper.

Acknowledgements

L. Hoyer acknowledges a Visiting Research Fellowship from the Institute for Rock Magnetism at the University of Minnesota and thanks

Dario Bilardello and Mike Jackson for their help whilst visiting the IRM. L. Hoyer acknowledges a free-standing NRF Scarce Skills Scholarship and Travel Grant. The authors thank Jiří Žák and Nick Schofield for their constructive reviews of this manuscript, anonymous reviewers for comments on a previous manuscript and Mike Watkeys for lively debates on similar topics.

Appendix A. Supplementary data

Supplementary data to this article can be found online at https://doi.org/10.1016/j.jvolgeores.2021.107427.

References

- Airoldi, G., Muirhead, J.D., White, J.D.L., Rowland, J., 2011. Emplacement of magma at shallow depth: insights from field relationships at Allan Hills, south Victoria Land, East Antarctica. Antarct. Sci. 23 (3), 281–296.
- Anderson, E.M., 1936. Dynamics of formation of cone-sheets, ring-dykes, and cauldron subsidence. Proc. Royal Soc. Edinburgh 56, 128–157.
- Anderson, E.M., 1951. The Dynamics of Faulting and Dyke Formation with Applications to Britain. Oliver and Boyd, Edinburgh, p. 206.
- Aragón, E., D'Eramo, F.J., Pinotti, L.P., Demartis, M., Tubía, J.M., Weinberg, R.F., Coniglio, J.E., 2018. Magma chamber growth models in the upper crust: a review of the hydraulic and inertial constraints. Geosci. Front. https://doi.org/10.1016/j.gsf.2018.10.005.
- Aubourg, C., Giordano, G., Mattei, M., Speranza, F., 2002. Magma flow in subaqueous rhyolitic dikes inferred from magnetic fabric analysis (Ponza Island, W. Italy). Phys. Chem. Earth Parts A/B/C 27 (25–31), 1263–1272.
- Aubourg, C., Tshoso, G., Le Gall, B., Bertrand, H., Tiercelin, J.J., Kampunzu, A.B., Dyment, J., Modisi, M., 2008. Magma flow revealed by magnetic fabric in the Okavango giant dyke swarm, Karoo igneous province, northern Botswana. J. Volcanol. Geotherm. Res. 170, 247–261.
- Baer, G., Beyth, M., Reches, Z.E., 1994. Dykes emplaced into fractured basement, Timna Igneous Complex, Israel. J. Geophys. Res. Solid Earth 99, 24039–24050.
- Benn, K., Allard, B., 1989. Preferred mineral orientations related to magmatic flow in ophiolite layered gabbros. J. Petrol. 30, 925–946.
- Borradaile, G.J., Gauthier, D., 2001. AMS-detection of inverse fabrics without AARM in ophiolite dikes. Geophys. Res. Lett. 28, 3517–3520.
- Borradaile, G.J., Gauthier, D., 2003. Interpreting anomalous fabrics in ophiolite dikes. J. Struct. Geol. 25, 171–182.
- Borradaile, G.J., Henry, B., 1997. Tectonic applications of magnetic susceptibility and its anisotropy. Earth-Sci. Rev. 42, 49–93.
- Burchardt, S., 2008. New insights into the mechanics of sill emplacement provided by field observations of the Njardvik Sill, Northeast Iceland. J. Volcanol. Geotherm. Res. 173, 280–288.
- Burke, K., Dewey, J.F., 1973. Plume-generated triple junctions: key indicators in applying plate tectonics to old rocks. J. Geol. 81, 406–433.
- Callot, J.P., Guichet, X., 2003. Rock texture and magnetic lineation in dykes: a simple analytical model. Tectonophysics 366, 207–222.
- Callot, J.P., Gurevitch, E., Westphal, M., Pozzi, J.-P., 2004. Flow patterns in the Siberian traps deduced from magnetic fabric studies. Geophys. J. Int. 156, 426–430.
- Cañón-Tapia, E., 2001. Factors affecting the relative importance of shape and distribution anisotropy in rocks: theory and experiments. Tectonophysics 340, 117–131.
- Cartwright, J., Hansen, D.M., 2006. Magma transport through the crust via interconnected sill complexes. Geology 34, 929–932.
- Catuneanu, O., Wopfner, H., Eriksson, P.G., Cairncross, B., Rubidge, B.S., Smith, R.M.H., Hancox, P.J., 2005. The Karoo basins of south-central Africa. J. Afr. Earth Sci. 43, 211–253.
- Chanceaux, L., Menand, T., 2016. The effects of solidification on sill propagation dynamics and morphology. Earth Planet. Sci. Lett. 43, 211–253.
- Coetzee, A., Kisters, A.F.M., 2017. Dyke-sill relationships in Karoo dolerites as indicators of propagation and emplacement processes of mafic magmas in the shallow crust. J. Struct. Geol. 97, 172–188.
- Coetzee, A., Kisters, A.F.M., 2018. The elusive feeders of the Karoo Large Igneous Province and their structural controls. Tectonophysics 747–748, 146–162.
- Cooke, M.L., Pollard, D.D., 1996. Fracture propagation paths under mixed mode loading within rectangular blocks of polymethyl methacrylate. J. Geophys. Res. Solid Earth 101, 3387–3400.
- Cooke, M.L., Mollema, P.N., Pollard, D.D., Aydin, A., 1999. Interlayer slip and joint localization in the East Kaibab Monocline, Utah: field evidence and results from numerical modelling. Geol. Soc. Lond., Spec. Publ. 169, 23–49.
- Cox, K.G., 1989. The role of mantle plumes in the development of continental drainage patterns. Nature 342, 873–877.
- Cox, K.G., 1992. Karoo igneous activity, and the early stages of the break-up of Gondwanaland. In: Storey, B.C., Alabaster, T., Pankhurst, R.J. (Eds.), Magmatism and the Causes of Continental Breakup. 68. Geological Society of London Special Publication, pp. 37–148.
- Cox, K.G., Macdonald, R., Hornung, G., 1967. Geochemical and petrographic provinces in the Karoo basalts of southern Africa. Am. Mineral. 52, 1451–1474.
- Curtis, M.L., Riley, T.R., Owens, W.H., Leat, P.T., Duncan, R.A., 2008. The form, distribution and anisotropy of magnetic susceptibility of Jurassic dykes in H.U. Sverdrupfjella, Drenning Maud Land, Antarctica. Implications for dyke swarm emplacement. J. Struct. Geol. 30, 1429–1447.

- Day, R.M., Fuller, M., Schmidt, V.A., 1977. Hysteresis properties of titanomagnetites: grain size and composition dependence. Phys. Earth Planet. Inter. 13, 260–267.
- Delaney, P.T., Pollard, D.D., 1981. Deformation of host rocks and flow of magma during growth of minette dikes and breccia-bearing intrusions near Ship Rock, New Mexico. US Geol. Surv. Prof. Pap. 1202 61 pp.
- Duncan, A.R., Erlank, A.J., Marsh, J.S., 1984. Regional geochemistry of the Karoo igneous province. In: Erlank, A.J. (Ed.), Petrogenesis of the Volcanic Rocks of the Karoo Province. 13. Geological Society of South Africa Special Publication, pp. 355–388.
- Duncan, R.A., Hooper, P.R., Rehacek, J., Marsh, J.S., Duncan, A.R., 1997. The timing and duration of the Karoo igneous event, southern Gondwanaland. J. Geophys. Res. 102, 18127–18138.
- Dunlop, D.J., 2002. Theory and application of the Day plot (Mrs/Ms versus Hcr/Hc): 2. Application to data for rocks, sediments and soils. J. Geophys. Res. 107 (B3), 2057. https://doi.org/10.1029/2001JB000487.
- Eales, H.V., Marsh, J.S., Cox, K.G., 1984. The Karoo Igneous Province: an introduction. Spec. Geol. Soc. South Afr. Spec. Publ. 13, 1–26.
- Elburg, M., Goldberg, A., 2000. Age and geochemistry of Karoo dolerite dykes from northeast Botswana. J. Afr. Earth Sci. 31, 153–161.
- Ellam, R.M., Carlson, R.W., Shirley, S.B., 1992. Evidence from Re–Os isotopes for plume–lithosphere mixing in Karoo flood basalt genesis. Nature 359, 718–721.
- Elliot, D.H., Fleming, 2000. Weddell triple junction: the principle focus of Ferrar and Karoo magmatism during initial breakup of Gondwana. Geology 28, 539–542.
- Ellwood, B.B., 1978. Flow and emplacement direction determined for selected basaltic bodies using magnetic susceptibility anisotropy measurements. Earth Planet. Sci. Lett. 41, 1270–1273.
- Erlank, A.J., 1984. Petrogenesis of the volcanic rocks of the Karoo province. Geol. Soc. South Afr. Spec. Publ. 13 395 pp.
- Ernst, R.E., Buchan, K.L., 1997. Giant radiating dyke swarms: Their use in identifying pre-Mesozoic large igneous provinces and mantle plumes. In: Mahoney, J., Coffin, M. (Eds.), Large Igneous Provinces: Continental, Oceanic, and Planetary Volcanism, AGU Geophys. Monographs. 100, pp. 297–333.
- Ernst, R.E., Head, J.W., Parfitt, E., Grosfils, E., Wilson, L., 1995. Radiating dyke swarms on Earth and Venus. Earth Sci. Rev. 39, 1–58. https://doi.org/10.1016/0012-8252(95) 00017-5.
- Ferraccioli, F., Jones, P.C., Curtis, M.L., Leat, P.T., 2005. Subglacial imprints of early Gondwana break-up as identified from high resolution aerogeophysical data over western Dronning Maud Land, East Antarctica. Terra Nova 17, 573–579.
- Francis, E.H., 1982. Emplacement mechanism of late Carboniferous tholeiite sills in northern Britain. J. Geol. Soc. Lond. 139, 1–20.
- Frankel, J.J., 1969. The distribution and origin of the Effingham Rock Type, a dolerite derivative of intermediate composition in natal and Zululand, South Africa. Geol. Soc. Am. Mem. 115, 149–174.
- Galerne, C.Y., Galland, O., Neumann, E., Planke, S., 2011. 3D relationships between sills and their feeders: evidence from the Golden Valley Sill Complex (Karoo Basin) and experimental modelling. J. Volcanol. Geotherm. Res. 202, 189–199.
- Galland, O., Bertelsen, H.S., Eide, C.H., Guldstrand, F., Haug, Ø.T., Leanza, H.A., Mair, K., Palma, O., Planke, S., Rabbel, O., Rogers, B.D., Schmiedel, T., Souche, A., Spacapan, J.B., 2018. Storage and transport of magma in the layered crust-Formation of sills and related flat-lying intrusions. In: Burchardt, S. (Ed.), Volcanic and Igneous Plumbing Systems. Elsevier, pp. 111–136.
- Galland, O., Spacapan, J.B., Rabbel, O., Mair, K., Soto, F.G., Eiken, T., Schiuma, M., Leanza, H.A., 2019. Structure, emplacement mechanism and magma-flow significance of igneous fingers Implications for sill emplacement in sedimentary basins. J. Struct. Geol. 124, 120–135.
- Geoffroy, L., Callot, J.P., Aubourg, C., Moreira, M., 2002. Divergence between magnetic and plagioclase linear fabrics in dykes: a new approach for defining the flow vector using magnetic foliation. Terra Nova 14, 183–190.
- Gröcke, D.R., Rimmer, S.M., Yoksoulian, L.E., Cairncross, B., Tsikos, H., van Hunen, J., 2009. No evidence for thermogenic methane release in coal from the Karoo-Ferrar large igneous province. Earth Planet. Sci. Lett. 277, 204–212.
- Gudmundsson, A., 2011. Deflection of dykes into sills at discontinuities and magmachamber formation. Tectonophysics 500, 50–64.
- Hansen, J., Jerram, D.A., McCaffrey, K., Passey, R., 2011. Early Cenozoic saucer-shaped sills of the Faroe Islands: an example of intrusive styles in basaltic lava piles. J. Geol. Soc. Lond. 168, 159–178.
- Hastie, W.W., Aubourg, C., Watkeys, M.K., 2011. When an 'inverse' fabric is not inverse: an integrated AMS-SPO study in MORB-like dykes. Terra Nova 23, 49–55.
- Hastie, W.W., Watkeys, M.K., Aubourg, C., 2014. Magma flow in dyke swarms of the Karoo LIP: implications for the mantle plume hypothesis. Gondwana Res. 25, 736–755.
- Henry, B., Jordanova, D., Jordanova, N., Souque, C., Robion, P., 2003. Anisotropy of magnetic susceptibility of heated rocks. Tectonophysics 366, 241–258.
- Horsman, E., Tikoff, B., Morgan, S.S., 2005. Emplacement-related fabric and multiple sheets in the Maiden Creek sill, Henry mountains, Utah, USA. J. Struct. Geol. 27, 1426–1444.
- Hoyer, L., Watkeys, M.K., 2016. Breccia formation during intrusion of a dolerite sill: an example from Sheffield Beach, KwaZulu-Natal North Coast, South Africa. S. Afr. J. Geol. 119, 663–676.
- Hoyer, L., Watkeys, M.K., 2017. Using magma flow indicators to infer flow dynamics in sills. J. Struct. Geol. 96, 161–175.
- Hutton, D.H.W., 2009. Insights into magmatism in volcanic margins: bridge structures and a new mechanism of basic sill emplacement - Theron Mountains, Antarctica. Pet. Geosci. 15, 269–278.
- Jamtveit, B., Svensen, H., Podladchikov, Y.Y., Planke, S., 2004. Hydrothermal vent complexes associated with sill intrusions in sedimentary basins. In: Breitkreucz, C., Petford, N. (Eds.), Physical Geology of High-Level Magmatic Systems. 234. Geological Society, London, Special Publications, pp. 233–241.

- Jelinek, V., 1978. Statistical processing of anisotropy of magnetic susceptibility measured on group of specimens, Stud. Geophys. Geod. 22, 50–62.
- Jelinek, V., 1981. Characterization of the magnetic fabric of rocks. Tectonophysics 79, 63–67
- Johnson, M.R., van Vuuren, C.J., Visser, J.N.J., Cole, D.I., 2006. In: de V Wickens, H., Christie, A.D.M., Roberts, D.L., Brandl, G., Johnson, M.R., Anhaeusser, C.R., Thomas, R.J. (Eds.), Sedimentary rocks of the Karoo Supergroup. The Geology of South Africa/Council for Geoscience. Geological Society of South Africa, pp. 461–500.
- Jolly, R.J.H., Sanderson, D.J., 1997. A Mohr circle construction for the opening of a preexisting fracture. J. Struct. Geol. 19, 887–892.
- Jourdan, F., Féraud, G., Bertrand, H., Kampunzu, A.B., Tshoso, G., Le Gall, B., Tiercelin, J.-J., Capiez, P., 2004. The Karoo triple junction questioned: evidence from the Jurassic and Proterozoic ⁴⁰Ar/³⁹Ar ages and geochemistry of the giant Okavango dyke swarm (Botswana). Earth Planet. Sci. Lett. 222, 989–1006.
- Jourdan, F., Féraud, G., Bertrand, H., Kampunzu, A.B., Tshoso, G., Watkeys, M.K., Le Gall, B., 2005. Karoo large igneous province: brevity, origin, and relation to mass extinction questioned by new ⁴⁰Ar/³⁹Ar age data. Geology 33, 745–748.
- Jourdan, F., Féraud, G., Bertrand, H., Watkeys, M.K., 2007. From flood basalts to the inception of oceanization: example from the ⁴⁰Ar/³⁹Ar high-resolution picture of the Karoo large igneous province. Geochem. Geophys. Geosyst. 8. https://doi.org/10.1029/2006GC001392, 20 pp.
- Jourdan, F., Féraud, G., Bertrand, H., Watkeys, M.K., Renne, P.R., 2008. The ⁴⁰Ar/³⁹Ar ages of the sill complex of the Karoo large igneous province: implications for the Pliensbachian-Toarcian climate change. Geochem. Geophys. Geosyst. 9 Q06009, 20 pp.
- Kattenhorn, S.A., Watkeys, M.K., 1995. Blunt-ended dyke segments. J. Struct. Geol. 17, 1535–1542.
- Kavanagh, J.L., Rogers, B.D., Boutelier, D., Cruden, A.R., 2017. Controls on sill and dyke-sill hybrid geometry and propagation in the crust: the role of fracture toughness. Tectonophysics 698, 109–120.
- Khan, M.A., 1962. Anisotropy of magnetic susceptibility of some igneous and metamorphic rocks. J. Geophys. Res. 67, 2873–2885.
- Klausen, M.B., 2009. The Lebombo monocline and associated feeder dyke swarm: diagnostic of a successful and highly volcanic rifted margin? Tectonophysics 468, 42–62.
- Knight, M.D., Walker, G.P.L., 1988. Magma flow directions in dikes of the Koolau Complex, Oahu, determined from magnetic fabric studies. J. Geophys. Res. 93, 4301–4319.
- Le Gall, B., Tshoso, G., Dyment, J., Kampunzu, A.B., Jourdan, F., Féraud, G., Bertrand, H., Aubourg, C., Vétel, W., 2005. The Okavango giant mafic dyke swarm (NE Botswana): its structural significance within the Karoo Large Igneous Province. J. Struct. Geol. 27, 2234–2255.
- Lensky, N.G., Niebo, R.W., Holloway, J.R., Lyakhovsky, V., Navon, O., 2006. Bubble nucleation as a trigger for xenolith entrapment in mantle melts. Earth Planet. Sci. Lett. 245, 278–288.
- Liss, D., Hutton, D.H.W., Owens, W.H., 2002. Ropy flow structures: a neglected indicator of magma-flow direction in sills and dikes. Geology 30, 715–718.
- Lister, J.R., Kerr, R.C., 1991. Fluid-mechanical models of crack propagation and their application to magma transport in dykes. J. Geophys. Res. 96, 10049–10077.
- Magee, C., Maharaj, S.M., Wrona, T., Jackson, C.A.L., 2015. Controls on the expression of igneous intrusions in seismic reflection data. Geosphere 11, 1024–1041.
- Magee, C., Muirhead, J.D., Karvelas, A., Holford, S.P., Jackson, C.A., Bastow, I.D., Schofield, N., Stevenson, C.T., McLean, C., McCarthy, W., 2016. Lateral magma flow in mafic sill complexes. Geosphere 12, 809–841.
- Magee, C., Muirhead, J.D., Schofield, N., Walker, R.J., Galland, O., Holford, S., Spacapan, J., Jackson, C.A.-L., McCarthy, W., 2018. Structural signatures of igneous sheet intrusion propagation. J. Struct. Geol. https://doi.org/10.1016/j.jsg.2018.07.010.
- Marsh, B., 2004. A magmatic mush column Rosetta Stone: the McMurdo dry valleys of Antarctica. EOS Trans. Am. Geophys. Union 47, 497–508.
- Marshall, C.G.A., von Brunn, V., 1999. The stratigraphy and origin of the Natal Group. S. Afr. J. Geol. 102, 15–25.
- Mekonnen, T.K., 2004. Interpretation and Geodatabase of Dykes Using Aeromagnetic Data of Zimbabwe and Mozambique. (Unpublished MSc. Thesis)International Institute for Geoinformation Science and Earth Observation, Enschede, The Netherlands 72 pp.
- Menand, T., 2011. Physical controls and depth of emplacement of igneous bodies: a review. Tectonophysics 500, 11–19.
- Muirhead, J.D., Airoldi, G., Rowland, J.V., White, J.D.L., 2012. Transport in the Ferrar large igneous province, Antarctica. Geol. Soc. Am. Bull. 124 (1-2), 162–180.
- Muirhead, J.D., Airoldi, G., Whitec, J.D.L., Rowland, J.V., 2014. Cracking the lid: sill fed dikes are the likely feeders of flood basalt eruptions. Earth Planet. Sci. Lett. 406, 187–197.
- Muirhead, J.D., Kattenhorn, S.A., Le Corvec, N., 2015. Varying styles of magmatic strain accommodation across the East African Rift. Geochem. Geophys. Geosyst. 16, 2775–2795.
- Nicholson, R., Pollard, D., 1985. Dilation and linkage of echelon cracks. J. Struct. Geol. 7, 583–590.
- Park, J.K., Tanczyk, E.I., Desbarats, A., 1988. Magnetic fabric and its significance in the 1400 Ma Mealy diabase dykes of Labrador, Canada. J. Geophys. Res. 93, 13689–13704.

- Paterson, S.R., Fowler Jr., T.K., Schmidt, K.L., Yoshinobu, A., Yuan, E.S., Miller, R.B., 1998. Interpreting magmatic fabric patterns in plutons. Lithos 44, 53–82.
- Peck, D.L., 1978. Cooling and vesiculation of Alae lava lake, Hawaii. USGS Professional Paper No. 935-B, pp. 1–49.
- Philpotts, A.R., Philpotts, D.E., 2007. Upward and downward flow in a camptonite dike as recorded by deformed vesicles and the anisotropy of magnetic susceptibility (AMS).

 I. Volcanol, Geotherm, Res. 161, 81–94
- Pollard, D.D., Muller, O.H., Dockstader, D.R., 1975. The form and growth of fingered sheet intrusions. Geol. Soc. Am. Bull. 86, 351–363.
- Pollard, D.D., Segall, P., Delaney, P.T., 1982. Formation and interpretation of dilatant echelon cracks. Geol. Soc. Am. Bull. 93, 1291–1303.
- Reeves, C.V., 1978. A failed Gondwana spreading axis in southern Africa. Nature 273, 222–223.
- Reeves, C.V., 2000. The geophysical mapping of Mesozoic dyke swarms in southern Africa and their origin in the disruption of Gondwana. J. Afr. Earth Sci. 30, 499–513.
- Rickwood, P., 1990. The anatomy of a dyke and the determination of propagation and magma flow directions. In: Parker, A.J., Rickwood, P.C., Tucker, D.H. (Eds.), Mafic Dykes and Emplacement Mechanisms. Balkema, Rotterdam, pp. 81–100.
- Riley, T.R., Curtis, M.L., Leat, P.T., Watkeys, M.K., Duncan, R.A., Millar, I.L., Owens, W.H., 2006. Overlap of Karoo and Ferrar magma types in KwaZulu-Natal, South Africa. I. Petrol. 47. 541–566.
- Rochette, P., Jackson, M., Aubourg, C., 1992. Rock magnetism and the interpretation of anisotropy of magnetic susceptibility. Rev. Geophys. 30, 209–226.
- Rochette, P., Aubourg, C., Perrin, M., 1999. Is this magnetic fabric normal? A review and case studies in volcanic formations. Tectonophysics 307, 219–234.
- Schofield, N., Stevenson, C., Reston, T., 2010. Magma fingers and host rock fluidization in the emplacement of sills. Geology 38, 63–66.
- Schofield, N.J., Brown, D.J., Magee, C., Stevenson, C.T., 2012a. Sill morphology and comparison of brittle and non-brittle emplacement mechanisms. J. Geol. Soc. 169, 127–141.
- Schofield, N., Heaton, L., Holford, S.P., Archer, S.G., Jackson, C.A.-L., Jolley, D.W., 2012b. Seismic imaging of 'broken bridges': linking seismic to outcrop-scale investigations of intrusive magma lobes. J. Geol. Soc. 169, 421–426.
- Schofield, N., Holford, S., Millett, J., Brown, D., Jolley, D., Passey, S.R., Muirhead, D., Grove, C., Magee, C., Murray, J., Hole, M., Jackson, C.A.L., Stevenson, C., 2015. Regional magma plumbing and emplacement mechanisms of the Faroe-Shetland Sill Complex: implications for magma transport and petroleum systems within sedimentary basins. Basin Res. 29, 41–63.
- Stephens, T.L., Walker, R.J., Healy, D., Bubeck, A., England, R., McCaffrey, K., 2017. Igneous sills record far-field and near-field stress interactions during volcano construction: Isle of Mull, Scotland. Earth Planet. Sci. Lett. 478, 159–174.
- Storey, B.C., 1995. The role of mantle plumes in continental breakup: case histories from Gondwanaland. Nature 377, 301–308.
- Storey, B.C., Alabaster, T., Hole, M.J., Pankhurst, R.J., Wever, H.E., 1992. Role of subductionplate boundary forces during the initial stages of Gondwana break-up: evidence from the proto-Pacific margin of Antarctica. Geol. Soc. Lond., Spec. Publ. 68, 149–163.
- Storey, B.C., Kyle, P.R., 1997. An active mantle mechanism for Gondwana breakup. South African Journal of Geology 100, 283–290.
- Svensen, H., Corfu, F., Polteau, S., Hammer, Ø., Planke, S., 2012. Rapid magma emplacement in the Karoo Large Igneous Province. Earth Planet. Sci. Lett. 325–326.
- Tarling, D.H., Hrouda, F., 1993. The Magnetic Anisotropy of Rocks. Chapman and Hall, London. p. 218.
- Tauxe, L., Gee, J., Staudigel, H., 1998. Flow directions in dike from anisotropy of magnetic susceptibility data: the bootstrap way. J. Geophys. Res. 103, 17775–17790.
- Thomson, K., Hutton, D., 2004. Geometry and growth of sill complexes: insights using 3D seismic from the North Rockall Trough. Bull. Volcanol. 66, 364–375. https://doi.org/10.1007/s00445-003-0320-z.
- Veevers, J.J., 2012. Reconstructions before rifting and drifting reveal the geological connections between Antarctica and its conjugates in Gondwanaland. Earth-Sci. Rev. 111, 249–318.
- Watkeys, M.K., 2002. Development of the Lebombo rifted volcanic margin of southeast Africa. In: Menzies, M.A., Klemperer, S.L., Ebinger, C.J., Baker, J. (Eds.), Volcanic Rifted Margins. Geological Society of America Special Paper. 362, pp. 27–46.
- White, R.S., 1997. Mantle Plume origin for the Karoo and Ventersdorp Flood Basalts, South Africa. S. Afr. J. Geol. 100, 271–283.
- White, R.S., McKenzie, D., 1989. Magmatism at rift zones: the generation of volcanic continental margins and flood basalts. J. Geophys. Res. 94, 7685–7729.
- Wilson, P.I.R., McCaffrey, K.J.W., Holdsworth, R.E., 2019. Magma-driven accommodation structures formed during sill emplacement at shallow crustal depths: the Maiden Creek sill, Henry Mountains, Utah. Geosphere 15, 1368–1392.
- Yoshinobu, A.S., Wolak, J.M., Paterson, S.R., Pignotta, G.S., Anderson, H.S., 2009. Determining relative magma and host rock xenolith rheology during magmatic fabric formation in plutons: examples from the middle and upper crust. Geosphere 5 (3), 270–285.